The Analysis of Multi-Clustering in Heavy Nuclei

by

Timothy Gary Carolus

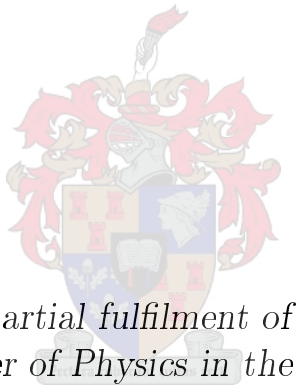

Thesis presented in partial fulfilment of the requirements for the degree of Master of Physics in the Faculty of Natural Science at Stellenbosch University

Supervisor: Prof. S.M. Wyngaardt
Co-supervisor: Dr. V. Malaza

March 2020

Declaration

By submitting this thesis electronically, I declare that the entirety of the work contained therein is my own, original work, that I am the sole author thereof (save to the extent explicitly otherwise stated), that reproduction and publication thereof by Stellenbosch University will not infringe any third party rights and that I have not previously in its entirety or in part submitted it for obtaining any qualification.

Date: March 2020

Abstract

The Analysis of Multi-Clustering in Heavy Nuclei

T.G. Carolus

Department of Physics,
University of Stellenbosch,
Private Bag X1, Matieland 7602, South Africa.

Thesis: MSc

March 2020

The binary cluster model is the simplest mathematical model which is used to describe a system of strongly interacting, and highly correlated nuclear matter. This study will serve as a means to better understand the phenomenon of nuclear clustering beyond a ^{208}Pb-alpha cluster core system. Theoretically predicted observables, such as the cluster decay half-life, positive parity cluster states, and the reduced electric dipole transition (B(E2)) are compared to the available experimentally observed quantities. The results show that the tested systems for various cluster-core configurations, of both a fixed parent nuclei and fixed stable core favoured the phenomenological description of their interaction. A numerical optimization procedure is applied to the core- cluster potential of the binary cluster formalism and is then used as an analytical tool in order to predict the possibility of higher modes of cluster decay in ^{216}Rn.

Uittreksel

Die ontleding van multi-bondeling in swaar kerne

("The Analysis of Multi-Clustering in Heavy Nuclei")

T.G. Carolus
Fisika Departement,
Universiteit van Stellenbosch,
Privaatsak X1, Matieland 7602, Suid Afrika.

Tesis: MSc

Maart 2020

Die binêre bondelmodel is die eenvoudigste wiskundige model wat gebruik word om 'n stelsel van sterk interaksie te beskryf, en sterk gekorreleerde kernmateriaal. Hierdie studie sal dien as 'n weg tot 'n beter verstaan van die verskynsel van kern groepering bo en behalwe 'n ^{208}Pb -alphagroepering kernstelsel. Teoreties voorspelbare waarneembares, soos die bondelvervalhalfleeftyd, positiewe bondelpariteitstoestande, en die verminderde elektriese dipooloorgang (B (E2)) word vergelyk met die beskikbare eksperimentele hoeveelhede. Die resultate toon dat toetsstelsels vir verskillende bondel-kernkonfigurasies, van beide die vaste ouer kern- en vaste stabiele kern skema, beter beskryf word deur die fenomenologiese beskrywing van hul wisselwerking.Numeriese optimering word toegepas op die kern-bondelpotensiaal van die binere bondel-formalisme, waarna dit as 'n analitiese instrument gebruik word vir die voorspelling van moontlike hoër modusse van bondelverval in ^{216}Rn

Acknowledgements

I would like to thank my thesis advisor, Prof. Shaun Wyngaardt for the introduction to the field of nuclear clustering and along with Dr Kimene Kaya for the guidance given in my research. With guidance in gain of the theoretical skills and development of numerical capabilities. Thanks to the Physics Department of Stellenbosch University for the opportunity to undertake my master studies. This was done under the financial assistance of ARMSCOR.

I would also like thank my fellow post-graduate students and classmates; Paul Williams, Frederick Waso, Andre De Bruyn, Scott Cameron and Imraan Badrodien for their morale support and guidance as former or current MSc students.

Finally, I would like to thank my parents, Gary and Penelopé and my sister, Gabriela for their support and guidance in managing social and academic life.

Contents

List of Figures

List of Tables

Chapter 1

Introduction

Nuclear matter is a strongly interacting many-body system, with nucleons interacting in a complex manner, these interactions cannot be solved exactly. Furthermore, the details behind nucleon-nucleon interactions, which determines the dynamical properties of the nucleus, are not fully understood and is therefore a key area of scientific investigation. It is understood that the nuclei is bound together due to an overall strong interaction between the nucleons. This interactions are short range and mainly occurring between neighbouring nucleons.These strong correlations amongst nucleons across such a large degree of freedom suggests some collective behaviour among subsets of nucleons within nuclei, which we define as a nuclear cluster state. Such simplifications in the nuclear model description is not without merit. The nuclear binding was determined by a Semi-empirical mass-formulae,[1] under the Liquid Drop Model. One of the first models used to describe the properties of nuclear matter is the Semi Empirical Mass Formula (SEMF). This model is obtained by fitting the parametrized SEMF formula

$$B(A,Z) = a_v A - a_s A^{2/3} - a_c \frac{Z^2}{A^{1/3}} + a_a \frac{(N-Z)^2}{4A} + \frac{\delta}{A^{1/2}}, \tag{1.0.1}$$

which depends on the volume(a_v), surface area(a_s), Coulomb repulsion(a_c), asymmetry between the protons and neutrons(a_a), and intrinsic spin pairing within a nucleus. The SEMF is essentially used to estimate the binding energy per nucleon for the nuclei found along the region of beta stability. The Liquid Drop Model assumed a uniform nucleon density for heavy stable nuclei. For the light nuclei the baryon density follows a Gaussian distribution. This formulation allows for the glimpse into the stability of the nucleus. When compared to the experimentally observed binding energies (see Figure 1), significant discontinuities can be found at specific proton and neutron numbers. These numbers are known as magic numbers as described by the Shell model [2] ,where the actual binding energy per nucleon is higher than for the neighbouring nuclei and in which the fermionic behaviour of the nucleons are taken into account.

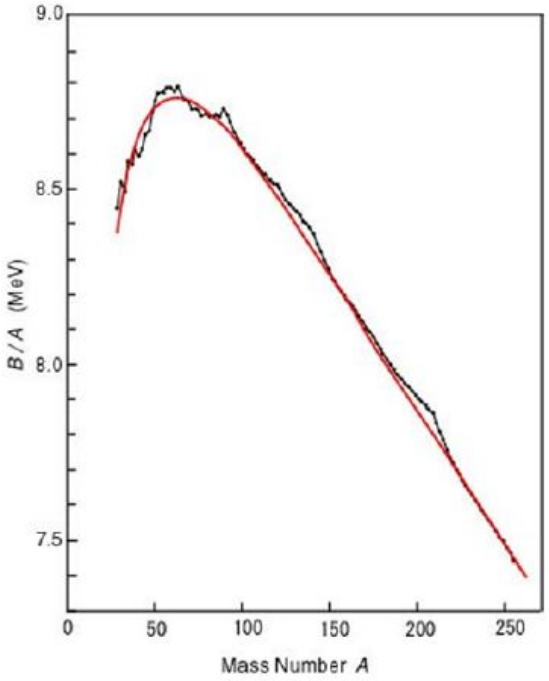

Figure 1.1: The difference in the actual(experimentally measured) binding energy (in Black) and the Liquid-Drop model estimate (in Red).

These nuclei are not always stable, whether it be in a natural or an induced state of excitation and would undergo decay to transition to a more stable configuration of nuclear matter. A variety of decay modes are known to achieve stability in nuclei, such as the emission of an electron or positron from the nucleus, which are referred to as beta (β) decay, the emission of neutrons, the emission of γ-rays or the emissions of a ^{4}He nuclei (also known as an α particle) namely α decay. The pioneering work of Rutherford, Geiger and Marsden in the early 1900s relied on the emission of alpha particles from alpha emitting nuclei, which resulted in the discovery of the atomic nucleus [3]. It was initially believed that alpha particles were the fundamental building blocks of the atomic nucleus, until the discovery of the proton in 1920 by Rutherford [4]. Alpha clustering in light nuclei have been observed experimentally [5] and have been studied in great detail, but differences in calculated binding energies and positive Q-values in heavy nuclei implied the possibility for the emission of a heavy cluster. Amongst the recent evidence of heavy clustering in nuclei is that of the ^{34}Si decay of ^{242}Cm, which maximized the decay Q-value due to strong shell effects[6].

The emission of single heavy cluster, beyond alpha clusters, has been investigated by du Toit et al [7]. As an independent particle, the stability of the cluster should be considered as well. This study will seek to look at beyond the single exotic clustering ,but to lay the foundations for a Lorentz covariant formalism to describe clustering phenomenon. In so doing, addressing the shortcomings of the microscopic description, gaining an understanding or the role of the nucleon-nucleon interaction in the clustering of heavy nuclei. With the focus being on multi-clustering , creating a means to distinguish between the expulsion of a single heavy cluster or the existence of multiple clusters and their decay modes is also of interest. This study seek to understand the mechanism surrounding the decay of ^{216}Rn, which could be considered as a ^{208}Pb core plus ^{8}Be cluster or ^{208}Pb core with two alpha clusters. It is well known that the free ^{8}Be is an unstable nucleus which decays via a double alpha decay with a decay half life of $10^{-16}s$ [8]. Questioning whether a weakly bound ^{8}Be may be emitted out of ^{216}Rn and then decay into 2 alpha particles or will the instability of the cluster dominate, favouring the release of 2 alpha particles via sequential decay. The latter opens up the possibility of viewing ^{216}Rn as a stable ^{208}Pb core with a multi-alpha like Bose-Einstein state. This approach will serve as benchmark for the study of stable core plus excited (or unstable) cluster or excited core plus stable cluster configurations.

1.1 Existing Theoretical Models

This section serves as a brief overview of some of the noteworthy theoretical cluster models, such as Fragmentation Theory, Asymmetric Two-Centre Shell Model(ATCSM), Analytical and Numerical Super-Asymmetric Fission Model. With the focus model of this this being the Binary Cluster Model (BCM). This section follows the structure as laid out in [9].

1.1.1 Fragmentation Theory

In order to describe the fragmentation process of a nucleus, the complete process is made of separate fragments , with a separation $\mathbf{R}$ from the centre-of-mass. Thus the collective Hamiltonian,$H(\mathbf{R}, \alpha_1, \alpha_2, \mu)$, in the coordinate system is parametrized in terms of the reduced mass of the cluster-core system μ, the deformation tensors of the respective fragments, α_1 and α_2 and the displacement vector $\mathbf{R}$.

Unfortunately, this theory does not describe joined or overlapping fragments and is treated with the Asymmetric Two-Centre Shell Model (ATCSM). The fragmentation model is used to describe fragmentation during nucleus-nucleus scattering, and has been successfully been applied to the study of nuclear decay of the description of nuclear clustering. With $H(\mathbf{R}, \alpha_1, \alpha_2, \mu)$

and adjustments made by the ATCSM, after renormalization of the model, the calculations are performed [10].

1.1.2 Asymmetric Two-Centre Shell Model(ATCSM)

In this model, the formation of fragments within the nucleus is theoretically constructed with an interaction potential which comprises of a superposition of two-oscillators, thus the name of two-centre shell model. The total Hamiltonian can be split into the following way:

$$H(\rho, z) = H_0 + V_1(\rho, z) + V_{LS} + V_{L^2}. \tag{1.1.1}$$

In the equation, H_0 is the Hamiltonian with two harmonic oscillator potentials, V_1 is a piecewise smoothing function for the oscillators with respect to separation distance z, between the core and cluster, and the V_{LS} and V_{L^2} are the spin-orbit coupling and total angular momentum dependent potentials. The Hamiltonian is defined in cylindrical coordinates z, ρ and ϕ. With the ρ being the radial distance with respect to the z axis, ϕ is the azimuthal angle and with the cluster and core placed along the z-axis, the z represents the separation distance between the cluster and core.

This model also employs smoothing of the functions joining the potential, as well as joining the potentials by variable heights of the potential barrier (as shown by figure 1.1.2), as to distinguish between the 2 fragments. Regardless of some it's successes, this model does not generalise well to complete asymmetric shaped nuclei as is present in exotic decay [11].

1.1.3 Analytical and Numerical Super-Asymmetric Fission Model

This model seeks to build upon the existing fission models [12; 13]. Through experimental observation and evidence of super-asymmetric fission or cluster decay, it is seen that current fission models overestimate the height of the fission barrier. Corrections to the fission barrier through the inclusion of a phenomenological adjustments, were taken into account in the Numerical (NuSAF) and Analytical (ASAF)Super-Asymmetric Fission models [14].

However, this is proven to a computationally intensive, means in order to solve this it requires a considerable amount of resources such as time, processing power or memory and as such an analytical relationship for the half-life was used as a starting point for the ASAF [15].

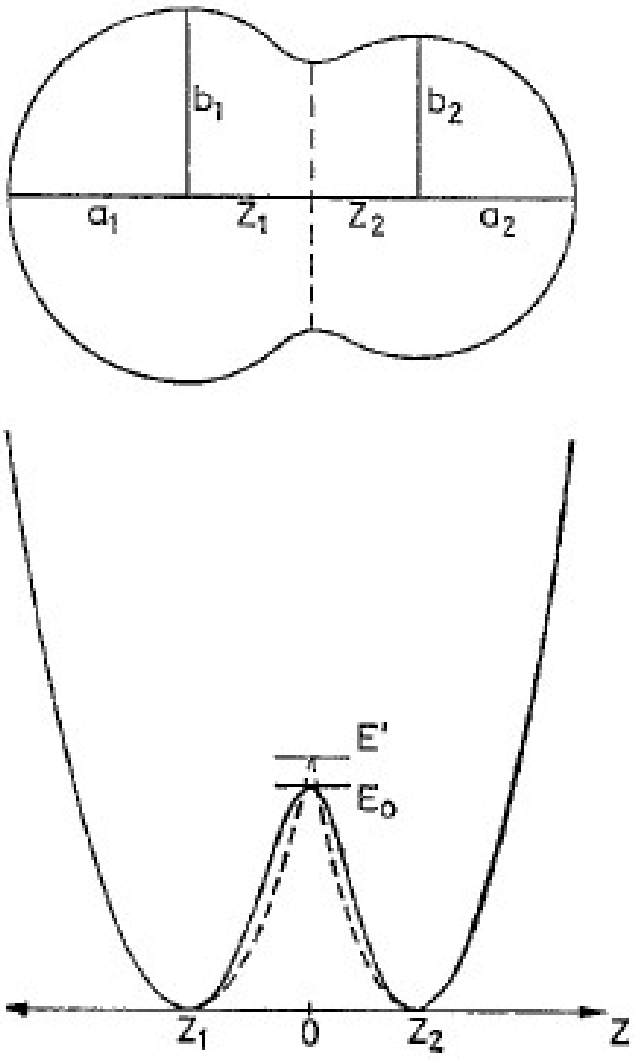

Figure 1.2: Visualisation of the Asymmetric Two-Centre Shell Model along the z-axis, with the centre-of-mass of the fragments at the roots (z_1 and z_2) of the potential $V(z, \rho)$. In which the z-axis represents the separation distance in fm and the vertical axis is in MeV. The image is visualized at a constant radial distance (ρ)[11].

1.1.4 Binary Cluster Model

The Binary Cluster Model (BCM) is the simplest of the cluster schemes discussed. This model begins with the assumption that the parent nucleus is made up of a cluster orbiting a core (see figure 1.3), separated by a distance r within the cluster-core centre-of-mass (CoM) coordinate system, interacting with one another by a central potential, which is composed of a Coulomb, centrifugal and nuclear potential. The BCM formalism assumes that mass asymmetry between the cluster and core is of such a nature that the CoM is

at the center of the core. The BCM will serve as the focus model with this work and will be explained further in chapter 2.

Whilst the fragmentation model assumes that the cluster and core already fragmented, the BCM can be considered for both nuclei in which the cluster and core are fragmented and configurations in which the nuclei matter at the core-cluster intersection overlaps. Allowing for the consideration of spherical and deformed nuclei. This models description of nuclear clustering has been used to predict the scattering as well as the bound state properties of clustering phenomenon.

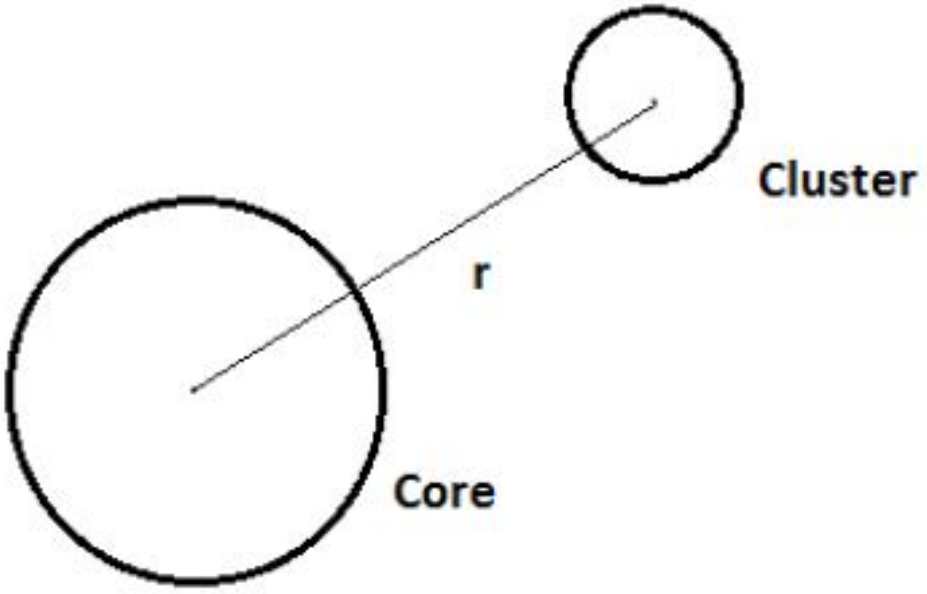

Figure 1.3: Graphical representation of the BCM.

1.2 Aim of the study

In this thesis, the focus model will be the Binary Cluster Model. Whilst investigating the effects of the a phenomenological and microscopic M3Y cluster-core potentials. Previously, theoretical cluster model studies focused solely on single cluster models. Such as the theoretical prediction[16] and the experimental verification [17] of the ^{14}C emission from ^{223}Ra. An extensive list of experimentally observed clustering presented in [6] ; for parent nuclei such as ^{221}Fr, $^{221-224,226}Ra$, $^{223,225}Ac$, $^{228,230}Th$, ^{231}Pa, $^{230,232-236}U$, $^{236,238}Pu$ and ^{242}Cm. In which single exotic clusters of ^{14}C, ^{20}O, ^{23}F, $^{22,24-26}Ne$, $^{28,30}Mg$, and $^{32,34}Si$ were detected. This study aims to apply these models to investigate the multi-cluster decay from nuclei, such as ^{216}Rn, which could be viewed as a ^{208}Pb core plus ^{8}Be cluster or ^{208}Pb core with two alpha clusters.

This thesis presents the ground for the theoretical formulation of the so called stable core plus excited cluster system. The theoretical predictions presented in this project will, however, be restricted to stable core and stable cluster systems, in which the ^{8}Be as a di-alpha system in ^{216}Ra is restricted to its ground state configuration. The current work also will consider the core in its ground state. This is done to bring the theory forth as an algorithmic tool for experimental predictions.

1.3 Plan of the thesis

The focus model of this thesis is the Binary Cluster Model and as such we will start by introducing the model. Thereafter, a look at various possibilities in the nuclear cluster-core potentials will be explored as to best describe the interaction between the Cluster-Core system. Starting with the phenomenological Saxon-Woods plus Saxon-Woods cubed potential, then a microscopic non-relativistic (M3Y) potential, after a comparison of these systems, a hybridization of these systems will be considered. Model shortcomings and absence of spin interactions will be considered.

Multi-configuration tests shall be run on each model. Finally, applications of these models as an investigative tool for multi-cluster decay study will be a conclusion this study.

Past iteration of the single cluster studies focused on either solely a phenomenological or microscopic interaction between the cluster and core. This study will also seek to incorporate more sophisticated representations of the microscopic potential. Laying the foundations for a model which describes the global properties of the nucleus, brought about by the phenomenological potential, whilst adding the nucleon-nucleon(NN) interactions and it's successes. The context, applications and adjustments to these interactions shall be expanded upon in chapter 3. Both the formalism and observables used for testing, looked at within the context of a decay process. Regardless of this,

as has done be the other models (section 1.1), this model and its extensions may be applied to tests under scattering process too. The resulting model will allow for the possible study of the structure of exotic nuclei through the use of radioactive ion beam (RIB) facilities.

Chapter 2

Binary Cluster Model

2.1 Introduction

In this chapter the theoretical foundation for binary cluster model is presented. The relevant model assumption is presented as well as the formalism for the relevant cluster observables, such as the positive parity excited energy states, electric multi-pole transition and decay half-life are given.

2.2 Model assumptions

The binary cluster model was first introduced in 1958 [18] by Wildermuth and Kanellopoulos. Within the model as presented by Buck et al. [19], a core with Z_1 protons and a mass of A_1 that is orbited by a cluster of Z_2 protons and a mass of A_2 to describe a parent nucleus where $Z = Z_1 + Z_2$ and $A = A_1 + A_2$ represents the total proton and mass numbers respectively.

It is assumed that the cluster-core system is a spherically symmetric system interacting through an effective central potential $V(r)$, in order to employ the use of center-of-mass coordinates between the cluster and core. The time independent Schrödinger equation (SE) for the cluster-core system under the aforementioned conditions is then given by

$$\left(-\frac{\hbar^2}{2\mu}\nabla^2 + V(r)\right)\psi(\mathbf{r}) = E\psi(\mathbf{r}), \tag{2.2.1}$$

where $\mathbf{r}$ is the position vector between the cluster and core, $\mu = \frac{A_1 A_2}{A_1+A_2}$ is the reduced mass, ψ is the bound state wave-function and E is the energy eigenvalue for the SE. As shall be seen in section 2.3, the cluster-core interaction is assumed to be spherically symmetric, thus the SE is calculated in spherical coordinates (r, θ, ϕ). With the Laplacian spherical coordinates taking the following form

$$\nabla^2 = \frac{1}{r^2}\frac{\partial}{\partial r}\left(r^2\frac{\partial}{\partial r}\right) + \frac{1}{r^2\sin\theta}\frac{\partial}{\partial\theta}\left(\sin\theta\frac{\partial}{\partial\theta}\right) + \frac{1}{r^2\sin^2\theta}\left(\frac{\partial^2}{\partial\phi^2}\right) \tag{2.2.2}$$

It should be noted that the vectors are in a bold font.

In solving the SE under a central potential $V(r)$, the bound state wave function of the relative motion is solved through the separation of variables into its radial and angular components as follows;

$$\psi_{nLM}(\mathbf{r}) = \frac{\varphi_{nL}(r)}{r} Y_{LM}(\theta, \phi) \tag{2.2.3}$$

where the radial component of the wave-function is represented by $\varphi_{nL}(r)$ and the angular component is represented by the spherical harmonic function, Y_{LM}. The quantum numbers are represented by n indicating the principle quantum number, L refers to the orbital angular momentum and the projection of orbital angular momentum onto the z-axis is represented by M. The radial and angular components of the SE is to be solved separately as it is assumed that the core-cluster interaction is spherically symmetric. The normalized angular wave functions are the spherical harmonics [20],

$$Y_{LM}(\theta, \phi) = (-1)^M \sqrt{\frac{(2L+1)}{4\pi} \frac{(L-|M|)!}{(L+|M|)!}} e^{iM\phi} P_{LM}(\theta, \phi) \tag{2.2.4}$$

here P_{LM} is the associated Legendre polynomial [21]. The spherical harmonics are eigenfunctions of the L^2 and L_z operators

$$L^2 Y_{LM} = L(L+1) Y_{LM} \tag{2.2.5}$$

$$L_z Y_{LM} = M Y_{LM} \tag{2.2.6}$$

and are orthonormal functions[1]

$$\int Y_{LM} Y_{L'M'} \, d\Omega = \delta_{LL'} \delta_{MM'}. \tag{2.2.7}$$

Substituting this into the SE yields,

$$\left(-\frac{\hbar^2}{2\mu} \nabla^2 + V(r) \right) \frac{\varphi_{nL}(r)}{r} Y_{LM}(\theta, \phi) = E_{nLM} \frac{\varphi_{nL}(r)}{r} Y_{LM}(\theta, \phi) \tag{2.2.8}$$

The SE can be reduced to the radial Schrödinger wave equation (RSE)

$$\left(-\frac{\hbar^2}{2\mu} \frac{d^2}{dr^2} + V(r) \right) \varphi_{nL}(r) = E_{nLM} \varphi_{nL}(r). \tag{2.2.9}$$

2.3 Cluster-Core Potential

The potential in the RSE can thus be thought as a composed of the nuclear potential $V_N(r)$, the Coulomb potential $V_c(r)$ and the centrifugal potential $V_L(r)$.

[1] The integration over the solid angle $d\Omega = \sin\theta \; d\theta d\phi$.

$$V(r) = V_N(r) + V_c(r) + V_L(r) \tag{2.3.1}$$

The Coulomb interaction is taken as a point charge of Z_2 to represent the cluster, which interacts with a uniformally charged core Z_1 with a radius of R_c. This description is expressed as follows;

$$V_c(r) = \begin{cases} \frac{Z_1 Z_2 e^2}{r} & \text{if } r \geq R_c, \\ \frac{Z_1 Z_2 e^2}{2R_c}\left(3 - |\frac{r}{R_c}|^2\right) & \text{if } r \leq R_c. \end{cases} \tag{2.3.2}$$

As to reduce the number of free parameters, the Coulomb radius R_C is taken as a nuclear radius $R_0 = 1.2A^{1/3}fm$ [22].

The centrifugal potential associated with the orbital angular momentum, with quantum number L, is given by

$$V_L(r) = \frac{L(L+1)\hbar^2}{2\mu r}, \tag{2.3.3}$$

where $\mu = \frac{A_1 A_2}{A_1 + A_2}$ is the reduced mass.

In the section to follow, an semi-classical approximation to the time-independent radial SE utilizing the Wentzel-Kramers-Brillouin (WKB) approximation [20; 23] shall be introduced. Langer [24] considered the solution under the influence of a Coulomb potential. He observed that the solution under this approximation was out of phase, and were corrected by replacing $L(L+1)$ with $(L+\frac{1}{2})^2$, as to ensure that the wave function is to vanish to the proper degree at $r = 0$. It is further stated that the discrepancy arises not in the method of solving the system but, in the application of the solution in the region approaching $r = 0$. This modification also takes into account the contribution from the $L = 0$ state within Bohr-Sommerfeld Quantization Rule [24].

The Langer modification of the centrifugal potential:

$$V_L(r) = \frac{(L+\frac{1}{2})^2\hbar^2}{2\mu r}. \tag{2.3.4}$$

2.4 Energy Spectra

2.4.1 Bohr-Sommerfeld Quantization

The Bohr-Sommerfeld Quantization serves as a semi-classical approximation to solving the one-dimensional Schrödinger Equation through the use of the semi-classical Wentzel-Kramers-Brillouin (WKB) approximation. The procedure that follows is taken from Griffiths [20], Zettili [23] and du Toit [7].

Now consider the one dimensional time independent Schrödinger equation

$$\left[-\frac{\hbar^2}{2\mu}\frac{d^2}{dr^2} + V(r)\right]\varphi = E\varphi \tag{2.4.1}$$

where $\mu = \frac{A_1 A_2}{A_1 + A_2}$ is the reduced mass of the core-cluster system. Through the introduction of the classical momentum $p(r) = \sqrt{2\mu(E - V(r))}$, the SWE can be rewritten as follows:

$$\frac{d^2}{dr^2}\varphi(r) + \frac{p^2(r)}{\hbar^2}\varphi = 0 \tag{2.4.2}$$

This method assumes that the potential is slow-varying with respect to r, and attempts to fit a solution of the form

$$\varphi(r) = A(r)e^{i\phi(r)/\hbar} \tag{2.4.3}$$

where $A(r)$ is the amplitude and $\phi(r)$ is the phase, which a both real valued functions. Or approximated by

$$\varphi(r)_{\pm} \approx \frac{C_{\pm}}{\sqrt{p(r)}} exp\left[\pm\frac{i}{\hbar}\int^{r} p(r')dr'\right] \tag{2.4.4}$$

This solution will be explored within both the classically forbidden ($V(r) > E$) and the classically allowed regions ($V(r) < E$), as this leads to two separate solutions.

Firstly, within the classically allowed region in which $E > V(r), r_1 < r < r_2$ in which $p(r)$ is a real function. The general solution is given by

$$\varphi(r) = \frac{C_+}{\sqrt{p(r)}} \exp\left[\frac{i}{\hbar}\int_{r_1}^{r_2} p(r')dr'\right] + \frac{C_-}{\sqrt{p(r)}} \exp\left[-\frac{i}{\hbar}\int_{r_1}^{r_2} p(r')dr'\right] \tag{2.4.5}$$

The classically forbidden, $V(r) > E$, yields a general solution of

$$\varphi(r) = \frac{B_+}{\sqrt{|p(r)|}} \exp\left[\frac{1}{\hbar}\int_{r} |p(r')|dr'\right] + \frac{B_-}{\sqrt{|p(r)|}} \exp\left[-\frac{1}{\hbar}\int_{r} |p(r')|dr'\right] \tag{2.4.6}$$

this is evaluated on either of the classically forbidden regions, namely from $r_{min} < r < r_1$ and for $r_2 < r < r_{max}$.

As mentioned above, the WKB approximation is valid if the potential or the wavelength λ of the particle is slow varying over distance, i.e.

$$|\frac{d\lambda}{dr}| \ll 1 \tag{2.4.7}$$

in which λ is defined as

$$\lambda(r) = \frac{\hbar}{p(r)} = \frac{\hbar}{\sqrt{2\mu(E - V(r))}} \tag{2.4.8}$$

this is the de Broglie wavelength of the cluster at distance r from the core. This condition is satisfied for classical systems, which breaks down at the turning points (or inflection points) $r = r_1$ and $r = r_2$, where $E = V(r)$ and the

momentum vanishes. The solutions previously introduced are not valid at the turning points. As such, the exact wave functions at the turning points need to be determined, and the matching conditions for the wave functions in the classically allowed and forbidden region.

Solutions within the classically forbidden are expected to decay exponentially, and solutions in the classically allowed region is to be oscillatory. This leads to three separate solutions;

$$\begin{aligned}
\varphi_1(r) &= \frac{C_1}{\sqrt{|p(r)|}} \exp\left[-\frac{1}{\hbar}\int_r^{r_1} |p(r')|dr'\right] \\
\varphi_2(r) &= \frac{C_2}{\sqrt{p(r)}} \sin\left(\frac{1}{\hbar}\int_{r_1}^{r_2} p(r')dr' + \alpha\right) \\
\varphi_3(r) &= \frac{C_3}{\sqrt{|p(r)|}} \exp\left[\frac{1}{\hbar}\int_{r_2}^{r} |p(r')|dr'\right]
\end{aligned} \tag{2.4.9}$$

where C_1, C_2 and C_3 are constants to be determined by connecting the solutions φ_1, φ_2 and φ_3 when moving from one region to the next as it passes the turning points $r = r_1$ and $r = r_1$, and α is a phase to be determined.

The Schrödinger equation can be solved approximately near $r = r_2$, by assuming the that potential can be expanded as a Taylor series about the point r_2. Expanding $V(r)$ to the first order

$$V(r) \approx V(r_2) + (r - r_2)\left(\frac{dV(r)}{dr}\right)|_{r=r_2}$$

where $V(r_2) = E$.
In this way, $V(r)$ is approximated by a straight line $(r - r_2)F_0$ with $F_0 = \left(\frac{dV(r)}{dr}\right)_{r=r_2}$ the slope of $V(r)$ at $r = r_2$. Applying a change of variables of the form $y = \left(\frac{2mF_0}{\hbar^2}\right)^{1/3}(r - r_2)$, the Schrödinger equation becomes

$$\frac{d^2\varphi(y)}{dy^2} - y\varphi(y) = 0$$

for which the solution is Airy functions $Ai(y)$ [21; 7]of the first kind

$$\varphi(y) = A'Ai(y) = \frac{A'}{\pi}\int_0^{\infty} \cos\left(\frac{z^3}{3}yz\right)dz \tag{2.4.10}$$

with A' as the normalization constant.

The asymptotic behaviour of Airy functions at both large positive and negative values of y, yields a wave function of the following form;

$$\varphi(y) = \begin{cases} \frac{A'}{\sqrt{\pi}|y|^{1/4}} \sin\left[\frac{2}{3}(-y)^{3/2} + \frac{\pi}{4}\right] & , y \ll 0 \\ \frac{A'}{2\sqrt{\pi}y^{1/4}} \exp\left[-\frac{2}{3}(y)^{3/2}\right] & , y \gg 0 \end{cases}$$

By using the following relation

$$\frac{1}{\hbar}\int_{r}^{r_2} p(r')dr' = \frac{2}{3}(-y)^{3/2} \tag{2.4.11}$$

the wave function becomes

$$\varphi(y) = \begin{cases} \frac{A}{\sqrt{p(r)}} \sin\left[\frac{1}{\hbar}\int_{r}^{r_2} p(r')dr' + \frac{\pi}{4}\right] & , r \ll r_2 \\ \frac{A}{2\sqrt{|p(r)|}} \exp\left[-\frac{1}{\hbar}\int_{r}^{r_2} p(r')dr'\right] & , r \gg r_2 \end{cases}$$

Following a similar procedure on either side of the turning point (inflection points) $r = r_1$ yields

$$\varphi(y) = \begin{cases} \frac{A'}{2\sqrt{|p(r)|}} \exp\left[-\frac{1}{\hbar}\int_{r_1}^{r} p(r')dr'\right] & , r \ll r_1 \\ \frac{A'}{\sqrt{p(r)}} \sin\left[\frac{1}{\hbar}\int_{r_1}^{r} p(r')dr' + \frac{\pi}{4}\right] & , r \gg r_1 \end{cases}$$

The oscillatory solutions for the region between r_1 and r_2, describes the same region and thus, must be equal.

$$\varphi_2(r) = \frac{A'}{\sqrt{p(r)}} \sin\left(\frac{1}{\hbar}\int_{r_1}^{r} p(r')dr' + \frac{\pi}{4}\right) = \frac{A}{\sqrt{p(r)}} \sin\left(\frac{1}{\hbar}\int_{r}^{r_2} p(r')dr' + \frac{\pi}{4}\right) \tag{2.4.12}$$

which my be likened to a simplified form of $A' \sin\theta_1 = A \sin\theta_2$ This equation is satisfied when the following two relations are met:

$$\theta_1 + \theta_2 = (n+1)\pi \tag{2.4.13}$$

$$A' = (-1)^n A \tag{2.4.14}$$

This leads to the well-known Bohr-Sommerfeld Quantization Rule

$$\int_{r_1}^{r_2} \sqrt{\frac{2\mu}{\hbar^2}(E_n - V(r))}dr = (2n+1)\frac{\pi}{2}. \tag{2.4.15}$$

This rule can be used to determine the quantized (WKB) energy levels E_n of the bound states of a semi-classical system, where n represents the number of nodes.

2.4.2 Global Quantum Number

The global quantum number is defined as:

$$G = 2n + L \tag{2.4.16}$$

where n and L are numbers of the node and orbital angular momentum characterizing the orbit.

This relation gives rise to a band of states which shares a common value of G. For even number G, the states form a band with positive parity states and an odd G yields a band of negative parity states.

For exotic decay, the global quantum number is to be proportional to the emitted cluster mass (A_2). The parametrization found to be optimal for nuclei within the actinide region is [25]

$$G = 5A_2. \tag{2.4.17}$$

Substituting equation 2.4.16 into the Born-Sommerfeld Rule given by equation 2.4.15

$$\int_{r1}^{r2} \sqrt{\frac{2\mu}{\hbar^2}(E_L - V_L(r))}dr = (G - L + 1)\frac{\pi}{2}. \tag{2.4.18}$$

With this in hand, the energy levels may be calculated if the potential $V_L(r)$ is known and the Global Quantum Number (G) is specified. This equation shall be implemented as part of a parameter optimization process.

2.4.3 Coupling to the electromagnetic field

In the nuclear decay process, the emission of a γ- ray occurs when the nucleus decays from an excited state to a lower state and is caused by the interaction of the nucleus with an external electromagnetic field. In this section, a brief derivation by means of a perturbation theory is presented and will be used to calculate the transition probabilities as accordance with Wong [26].

Firstly, consider a point particle with a charge of **q**. The free Hamiltonian for a particle in the absence of an external electromagnetic field and consisting of only a kinetic energy term with a momentum of **p** and mass m;

$$H_0 = \frac{1}{2m}\mathbf{p}^2. \tag{2.4.19}$$

In the presence of an electromagnetic field, the momentum gets modified as follows

$$\mathbf{p} \rightarrow \mathbf{p} + \frac{\mathbf{q}}{c}\mathbf{A}$$

where **A** is the vector potential for the electromagnetic field. The general form of the Hamiltonian can be expressed in the form of a current J. Written in a more convenient four- component tensor notation looks as follows,

$$H' = -\frac{1}{c}\sum_{\mu=1}^{4} A_\mu J_\mu \tag{2.4.20}$$

where $A_\mu = (\mathbf{A}, iV)$ and $J_\mu = (\mathbf{J}, i\rho c)$ with a charge density of $\mathbf{J} = q\frac{\mathbf{p}}{m}$. The form of the electromagnetic field is given by the solution of Maxwell's equations,

$$\left(\nabla^2 - \frac{1}{c^2}\frac{\partial^2}{\partial t^2}\right) A_r(\mathbf{r}, t) = 0 \tag{2.4.21}$$

As our interest is the vector potential A_μ, this can be written with the time dependence removed in terms of a definite wave number $\mathbf{k}$,

$$\mathbf{A}(\mathbf{r},t) = \sum_i \sum_{k_i} A_{k_i}(\mathbf{r}) e^{-i\omega_i t} \tag{2.4.22}$$

where $\omega = kc$, with k being the magnitude of $\mathbf{k}$. The spatial dependence of $\mathbf{A}$ is then given by

$$(\nabla^2 + k^2)\mathbf{A}_\mathbf{k}(\mathbf{r}) = 0 \tag{2.4.23}$$

Substituting the expansion into the above solution yields,

$$\mathbf{A}(\mathbf{r},t) = \frac{1}{N} \sum_k \sum_\eta \left(\mathbf{b}_{\mathbf{k}\eta} \epsilon_\eta e^{i(\mathbf{k}\cdot\mathbf{r}-\omega t)} + \mathbf{b}^\dagger_{\mathbf{k}\eta} \epsilon_\eta e^{-i(\mathbf{k}\cdot\mathbf{r}-\omega t)} \right) \tag{2.4.24}$$

From the condition $\nabla \cdot \mathbf{A} = 0$, only two of the three components for the vector field are independent. These components are indicated by two unit vectors ϵ_η with $\eta = 1, 2$, indicating the polarization of the photon. The factors $\mathbf{b}_{\mathbf{k}\eta}$ and $\mathbf{b}^\dagger_{\mathbf{k}\eta}$ are constants related to the boundary conditions. A quantum-mechanical interpretation of $\mathbf{b}_{\mathbf{k}\eta}$ and $\mathbf{b}^\dagger_{\mathbf{k}\eta}$ is that they represent the creation and annihilation operators, respectively, of photons with wave-number $\mathbf{k}$ and polarization direction η.

The expansion solution for $\mathbf{A}$ is implicitly done in Cartesian coordinates, but since our model assumes spherical symmetry, it is more convenient to express $\mathbf{A}(\mathbf{r},t)$ in terms of definite spherical tensor. This coordinate change allows for $\mathbf{A}(\mathbf{r},t)$ to be written in terms of eigenfunctions of the angular momentum operator such that

$$\begin{aligned} \mathbf{J}^2 \mathbf{A}_{\lambda\mu}(\mathbf{r},t) &= \lambda(\lambda+1)\mathbf{A}_{\lambda\mu}(\mathbf{r},t) \\ \mathbf{J_0} \mathbf{A}_{\lambda\mu}(\mathbf{r},t) &= \mu \mathbf{A}_{\lambda\mu}(\mathbf{r},t). \end{aligned}$$

The functions $\mathbf{A}_{\lambda\mu}$ may be expressed in terms of *vector spherical harmonics*, which are vector functions constructed from (scalar) spherical harmonics $Y_{lm}(\theta,\phi)$.

$$\mathbf{A}_{\lambda\mu}(\mathbf{r},t) = f_\lambda(kr) Y_{\lambda\mu} e^{-i\omega t} \tag{2.4.25}$$

Standing wave solutions to the radial function $f_\lambda(kr)$ is that of the spherical Bessel function, $j_\lambda(kr)$. For outgoing and incoming propagating solutions are $h^{(1)}_\lambda(kr)$ and $h^{(2)}_\lambda(kr)$, which are the spherical Hankel functions of the 1^{st} and 2^{nd} kind respectively [27].

The introduction of the orbital angular momentum operator defined within the angular coordinates,θ and ϕ

$$\mathbf{L} = -i\mathbf{r} \times \nabla. \tag{2.4.26}$$

Applying this operator to $\mathbf{A}_{\lambda\mu}(\mathbf{r},t)$ results in two vector field solutions

$$\begin{aligned} \mathbf{L}\mathbf{A}_{\lambda\mu}(\mathbf{r},t) &= -i(\mathbf{r}\times\nabla) f_\lambda(kr) Y_{\lambda\mu}(\theta,\phi) e^{i\omega t} \\ (\nabla \times \mathbf{L})\mathbf{A}_{\lambda\mu}(\mathbf{r},t) &= -i\nabla \times (\mathbf{r}\times\nabla) f_\lambda(kr) Y_{\lambda\mu}(\theta,\phi) e^{i\omega t}. \end{aligned}$$

These two solutions correspond to two different multipoles, namely that of the electric ($E\lambda$) and magnetic ($M\lambda$) multipole transitions. As written them in terms of spherical harmonics

$$\begin{aligned}\mathbf{A}_{\lambda\mu}(M\lambda,\mathbf{r},t) &= \frac{-i}{[\lambda(\lambda+1)]^{1/2}}(\mathbf{r}\times\nabla)(j_\lambda(kr)Y_{\lambda\mu})e^{-i\omega t}\\ \mathbf{A}_{\lambda\mu}(E\lambda,\mathbf{r},t) &= -\frac{-i}{[k\lambda(\lambda+1)]^{1/2}}\nabla\times(\mathbf{r}\times\nabla)(j_\lambda(kr)Y_{\lambda\mu})e^{-i\omega t}.\end{aligned}$$

Writing the perturbing Hamiltonian H' in terms of multipole operators, which is achieved through the introduction of electric and magnetic multipole operators written in terms of the above definition for $\mathbf{A}_{\lambda\mu}(E\lambda,\mathbf{r})$ and $\mathbf{A}_{\lambda\mu}(M\lambda,\mathbf{r})$ [26]

$$\begin{aligned}\mathbf{O}_{\lambda\mu}(E\lambda) &= -i\frac{(2\lambda+1)!!}{ck^{\lambda+1}(\lambda+1)}\mathcal{J}(\mathbf{r})\cdot\nabla\times(\mathbf{r}\times\nabla)(j_\lambda(kr)Y_{\lambda\mu}))\\ \mathbf{O}_{\lambda\mu}(M\lambda) &= -\frac{(2\lambda+1)!!}{ck^{\lambda+1}(\lambda+1)}\mathcal{J}(\mathbf{r})\cdot(\mathbf{r}\times\nabla)(j_\lambda(kr)Y_{\lambda\mu})),\end{aligned}\tag{2.4.27}$$

which are both spherical tensors of rank λ.

The nuclei of interest to this study, are typically smaller than 10 fm. Furthermore, the energies attributed to gamma rays, E_γ, are generally less than 10 MeV, which results in a wave number of $k = E_\gamma/\hbar c \approx 1/20 fm^{-1}$ or less. Since the product of kr is less than 1, the (scalar) radial function, Bessel function, may be approximated to first order

$$j_\lambda(kr) \approx \frac{(kr)^\lambda}{(2\lambda+1)!!}\left(1-\frac{1}{2}\frac{(kr)^2}{2\lambda+3}+\cdots\right),\tag{2.4.28}$$

which is also known as a long-wavelength limit.

Through the use of this long wavelength limit, and the assumption of the electric contribution originating from a point charge of the protons

$$\begin{aligned}\mathbf{O}_{\lambda\mu}(E\lambda) &= \sum_{i=1}^{A} e(i)r_i^\lambda Y_{\lambda\mu}(\theta_i,\phi_i)\\ \mathbf{O}_{\lambda\mu}(M\lambda) &= \sum_{i=1}^{A}\left(g_s(i)s_i + g_l(i)\frac{2l_i}{\lambda+1}\right)\cdot\nabla_i(r_i^\lambda Y_{\lambda\mu}(\theta_i,\phi_i))\end{aligned}\tag{2.4.29}$$

where $e(i) = 1e$ or $e(i) = 0$ for protons and neutrons respectively.

The transition probabilities (per unit time) are calculated through the use of *Fermi's Golden Rule*

$$\mathcal{W} = \frac{2\pi}{\hbar}|\left\langle\phi_f(\mathbf{r})\right|H'\left|\phi_i(\mathbf{r})\right\rangle|^2\rho(E_f).\tag{2.4.30}$$

By inserting the multipole operators into equation 2.4.30 and considering the density of final states ($\rho(E_f)$) to be proportional to the nuclear matrix elements, allows us to write the transition probability for multipole λ from initial state $|J_i M_i\rangle$ to final state $\langle J_f M_f|$ as follows,

$$\mathcal{W}(\lambda; J_i \to J_f) = \frac{8\pi(\lambda+1)}{\lambda[(2\lambda+1)!!]^2}\frac{k^{2\lambda+1}}{\hbar}B(\lambda; J_i \to J_f), \tag{2.4.31}$$

in which $B(\lambda; J_i \to J_f)$ is the reduced transition probability give in terms of reduced matrix elements as

$$\begin{aligned} B(\lambda; J_i \to J_f) &= \sum_{\mu M_f} |\langle J_f M_f| \mathbf{O}_{\lambda\mu} |J_i M_i\rangle|^2 \\ &= \frac{1}{2J_i+1}|\langle J_f| \mathbf{O}_{\lambda} |J_i\rangle|^2. \end{aligned} \tag{2.4.32}$$

2.5 Reduced Electromagnetic Transitions

It is often more useful and computationally efficient to look at the reduced transition probability. As there are an abundance of experimental data pertaining to the electric transition, especially that of low lying transitions, we will only focus on electric transitions.

It should be noted that in the derivation in section 2.4.3, λ referred to the angular momentum and thus, an appropriate relabelling to l is needed for this context and similarly, for μ , which refers to the projection of the angular momentum and shall be labelled m.

The electric operator, $\mathbf{O}_{lm}(El)$, is to be summed over the two total charges Z of the cluster and core [28]; ,

$$\begin{aligned} \mathbf{O}_{lm}(El) &= \sum_{i=1}^{Z} e(i) r_i^l Y_{lm}(\theta_i, \phi_i) \\ &\approx Z_1 r_1^l Y_{lm}(\theta_1, \phi_1) + Z_2 r_2^l Y_{lm}(\theta_2, \phi_2) \\ &= Z_1 r_1^l Y_{lm}(\pi-\theta, \pi+\phi) + Z_2 r_2^l Y_{lm}(\theta, \phi) \\ &= [(-1)^l Z_1 r_1^l + Z_2 r_2^l] Y_{lm}(\theta, \phi) \\ &= \left[Z_1 \left(-\frac{A_2 r}{A}\right)^l + Z_2 \left(\frac{A_1 r}{A}\right)^l \right] Y_{lm}(\theta\phi) \\ &= \left[Z_1 \left(-\frac{A_2}{A}\right)^l + Z_2 \left(\frac{A_1}{A}\right)^l \right] r^l Y_{lm}(\theta\phi) \\ &= \beta_l r^l Y_{lm}(\theta, \phi) \end{aligned} \tag{2.5.1}$$

in the above, the behaviour of spherical harmonics under change of parity, then changed it to centre of mass coordinate and finally, presented the operator with

short hand notation

$$\beta_l = \left[Z_1 \left(-\frac{A_2}{A} \right)^l + Z_2 \left(\frac{A_1}{A} \right)^l \right]. \tag{2.5.2}$$

Reduced transition probability for an arbitrary transition

Electric multipole transitions of order from an initial state $|L_i M_i\rangle$ to a final state of $|L_f M_f\rangle$ is generalised as follows

$$\begin{aligned}
B(l; L_i \to L_f) &= \sum_{mM_f} |\langle L_f M_f| \mathbf{O_{lm}}(El) |L_i M_i\rangle|^2 \\
&= \sum_{mM_f} |\langle L_f M_f| \beta_l r^l Y^*_{lm}(\theta,\phi) |L_i M_i\rangle|^2 \\
&= \sum_{mM_f} |(-1)^m \langle L_f M_f| \beta_l r^l Y^*_{l-m}(\theta,\phi) |L_i M_i\rangle|^2 \\
&= \sum_{mM_f} |\langle L_i M_i l - m | L_f M_f\rangle|^2 |\langle L_f| |\beta_l r^l Y_l| |L_i\rangle|^2 \\
&= \sum_{mM_f} \frac{2L_f+1}{2L_i+1} |\langle L_i M_i l m | L_f M_f\rangle|^2 |\langle L_f| |\beta_l r^l Y_l| |L_i\rangle|^2 \\
&= \frac{2L_f+1}{2L_i+1} |\langle L_f| |\beta_l r^l Y_l| |L_i\rangle|^2 \\
&= \left(\frac{\hat{L}_f}{\hat{L}_i} \right)^2 |\langle L_f| |\beta_l r^l Y_l| |L_i\rangle|^2
\end{aligned} \tag{2.5.3}$$

Above the properties of the spherical harmonics under parity change, the Wigner-Eckart Theorem, symmetry and completeness relations of Clebsch-Gordan coefficients have been used [23; 29]. As well as the introduction short-hand operator $\hat{L} = \sqrt{2L+1}$.

The evaluation of the reduced matrix element is illustrated in [30] as follows

$$\begin{aligned}
|\langle L_f| |\beta_l r^l Y_l| |L_i\rangle|^2 &= (-1)^{2l} \sum_{M'q} \langle L_i M' l q | L_f M\rangle \langle L_f M| \beta_l r^l Y_{lq} |L_i M'\rangle \\
&= (-1)^{2l} \sum_{M'q} \langle L_i M' l q | L_f M\rangle \langle \psi_{L_f} Y_{L_f M}| \beta_l r^l Y_{lq} |\psi_{L_i} Y_{L_i M'}\rangle \\
&= (-1)^{2l} \sum_{M'q} \langle L_i M' l q | L_f M\rangle \langle \psi_f| \beta_l r^l |\psi_i\rangle \langle Y_{L_f M}| Y_{lq} |Y_{L_i M'}\rangle \\
&= (-1)^{2l} \sum_{M'q} \langle L_i M' l q | L_f M\rangle \langle \psi_f| \beta_l r^l |\psi_i\rangle \langle L_i M' l q | L_f M\rangle \langle L_f| |Y_l| |L_i\rangle \\
&= \langle \psi_f| \beta_l r^l |\psi_i\rangle \langle L_f| |Y_l| |L_i\rangle \\
&= \left[\frac{(2L_i+1)(2l+1)}{4\pi(2L_f+1)} \right]^{1/2} \langle L_i 0 l 0 | L_f 0\rangle \langle \psi_f| \beta_l r^l |\psi_i\rangle
\end{aligned} \tag{2.5.4}$$

After the above procedure has been done, the reduced transition probability between arbitrary states can be written as

$$B(El; L_i \to L_f) = \frac{1}{4\pi}\beta_l^2 l^2 |\langle L_i 0 l 0 | L_f 0 \rangle|^2 |\langle \psi_f | r^l | \psi_i \rangle|^2 \tag{2.5.5}$$

2.6 Decay half-life

The decay half life is defined as the time taken to halve the number of radioactive nuclei in a sample. Mathematically represented in the form of

$$T_{1/2} = \frac{\hbar \ln 2}{\Gamma} \tag{2.6.1}$$

where the Γ is the decay width. The decay width for the break up of the cluster and core is defined as the product of the assault frequency F, the cluster-core preformation probability P and the penetrability of the cluster through the potential barrier T [31; 32; 33; 34]

$$\Gamma = \hbar PFT \tag{2.6.2}$$

The assault frequency F is given by [5]

$$F = \frac{\hbar}{2\mu \int_{r_1}^{r_2} dr \frac{1}{k(r)}} \tag{2.6.3}$$

and $k(r)$ is the wave number

$$k(r) = \sqrt{\frac{2\mu}{\hbar^2}|E - V(r)|}. \tag{2.6.4}$$

The penetrability is determined by the ratio of the transmitted flux to the incident flux densities of the tunnelling process through the potential barrier[23]. When a WKB approximation is applied to the penetrability at the turning (inflection) points of the potential [33] and generalised to three dimensions, it yields

$$T = \exp\left(-2\int_{r_2}^{r_3} k(r)dr\right). \tag{2.6.5}$$

The physical process associated with the above equation is the so called tunnelling effect. Putting all these components together gives rise to the following form

$$\Gamma = P\frac{\hbar^2}{2\mu}\frac{\exp\left(-2\int_{r2}^{r3} k(r)dr\right)}{\int_{r1}^{r2} dr \frac{1}{k(r)}} \tag{2.6.6}$$

where $\mu = \frac{A_1 A_2}{A_1 + A_2}$ is the reduced mass, in terms of the core mass A_1 and cluster mass A_2.

The only quantity not defined is the pre-formation probability P, which is the probability of a preformed cluster-core system in the initial state. This quantity can be explicitly determined from a microscopic shell model [35; 36]. In the initial calculation of the half-lives, the model is calculated under the assumption that the cluster and core is in it's ground state. This is done with the energy E taken to be the Q-value, $P = 1$ and the governing potential $V(r)$ taken at the L = 0 state. The calculated half-life is then fitted to the experimental value, as to adjust pre-formation probability.

Final remarks

In this chapter, the basic model assumptions of the BCM and the formalism of the relevant BCM observables, has been presented. A key quantity which appears on all the predicted cluster observables is the core cluster potential. In Chapter 4, various core-cluster potentials are presented. For this thesis work, there will be a specific focus on the phenomenological cubic Saxon-Woods potential, the double folded M3Y potential as well as the newly formulated Hybrid potential.

Chapter 3

Nuclear Cluster Potentials

3.1 Introduction

Chapter 2 has introduced the model assumptions in terms of the Hamiltonian describing the geometry of the cluster-interactions and the observables that will be used in the analysis process. The total potential presented did not include the nuclear potential V_N and its contribution to describing the structure of nuclear matter.

The following potentials have been used in the past to varying degrees of success. Each of which have a different levels of geometric/parametric complexities to consider. Starting with the introduction of the phenomenological model to incorporate global properties of the nucleus. A double-folding microscopic model is introduced to add the contributions from the nucleon-nucleon interactions. A comparison of these descriptions and there shortcomings shall be provided, along with a model that may build upon the strengths of these two models.

Square Well Potential

This is a simple potential with a form familiar to introductory quantum mechanics

$$V_N(r) = \begin{cases} -V_0 & \text{if } r \leq R_0 \\ 0 & \text{if } r > R_0 \end{cases} \tag{3.1.1}$$

where V_0 is the depth of the square well and R_0 it the radius. When used alongside a surface-charge Coulomb potential, this combination yields the α-decay half of even-even heavy nuclei to a factor of 2 [37].

Unfortunately, regardless of the simplicity of the fitting a square well potential, it will not be used due to it's inability to describe exotic decay process (i.e. beyond alpha decay).

3.2 Phenomenological potential

The phenomenological Saxon-Woods (SW) potential is defined as follows

$$V_N(r) = -V_0 \left[\frac{1}{1 + \exp(\frac{r-R}{a})} \right] \tag{3.2.1}$$

with the depth of the potential being represented by V_0, along with **a** being the diffuseness and R is the nuclear radius. Here the functional form reflects a two-parameter Fermi distributions for the nuclear density. The SW potential is often used in independent single particle shell model predictions. A physically reasonable geometry of the distribution is one in which the parameters are $R \sim A^{1/3}$ fm [1], where A is the mass number and $a \sim 0.65$ fm.

In light nuclei, the SW potential results in a degenerate or inverted energy spectra for alpha cluster states. Furthermore, the SW potential also fails at describing [38] the observation of anomalous large back angle scattering (ALAS) of alpha particles by closed shell nuclei. Correction to the differential cross-section, at backwards angles, was described by a SW2 Michel potential [39]. Another successful potential is that of the "cosh" potential; defined as

$$V_N(r) = -V_0 \frac{1 + \cosh(R_0/a)}{\cosh(r/a) + \cosh(R_0/a)} \tag{3.2.2}$$

Which saw many success in reproducing the half lives of α decay [22],[40] and [41]. The shortcoming of this potential being the inability to reproduce exotic decay data from odd-A nuclei [42]

This Saxon-Woods plus Saxon-Woods Cubed potential ($\mathbf{SW + SW^3}$) potential is of the form:

$$V_N = -V_0 \left[\frac{x}{1 + exp\left[\frac{(r-R_0)}{a}\right]} + \frac{1-x}{(1 + exp\left[\frac{(r-R_0)}{a}\right])^3} \right] \tag{3.2.3}$$

Consisting of the same parameters as the SW potential but, also introducing a mixing parameter x which indicates the relative contributions from the Wood-Saxon and cubic Wood-Saxon terms. When the mixing parameter is equal to 1, it returns the SW potential, this is visualised in figure 3.1. This is the form of the phenomenological potential to be used in this study.

Reproducing consistent results with regards to the level structure decay and scattering properties compared to available data [25; 5]. Microscopic nature of clustering is not revealed.

[1] The nuclear radius is the same as used in equation 2.3.2.

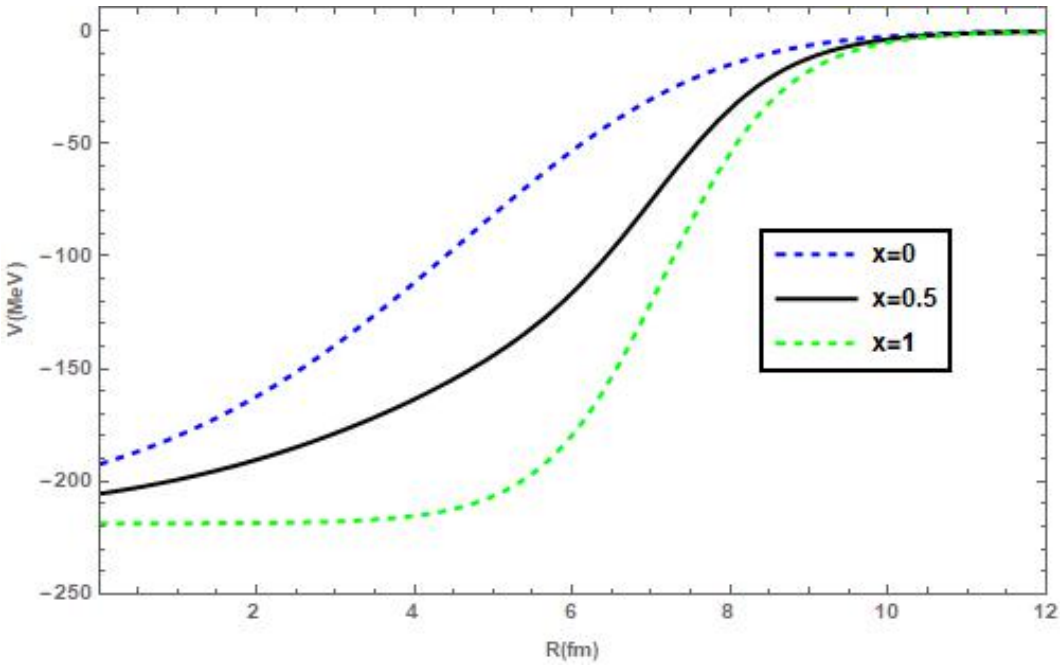

Figure 3.1: Illustration of the effects of the mixing parameter on the $SW + SW^3$ potential is shown for x equal to 0, 0.5 and 1.

3.3 Microscopic Non-relativistic Nuclear Potential

3.3.1 Double-Folded Model for Nuclear Cluster-Core Potential with the effective M3Y interaction

Note for this section Hat notation is used to represent the operators throughout the derivation of this potential model. Consider the bound cluster-core system as a projectile- target system in their ground states with the stationary SWE given by :

$$\hat{H}\Psi = E\Psi, \tag{3.3.1}$$

where H is the total Hamiltonian of the system, here the spin and isospin coordinates have been suppressed. Furthermore, the total Hamiltonian is defined as

$$\hat{H} = \hat{H}_A + \hat{H}_B + \hat{T}_0 + \sum_{ij} v(r_{ij}) \tag{3.3.2}$$

where $\hat{H}_A$ and $\hat{H}_B$ are the intrinsic Hamiltonians of the target and the projectile, $\hat{T}_0$ is the relative kinetic energy of the projectile with respect to the target and the interaction potential between projectile and target nucleons i and j is given by $v(r_{ij})$.

Suppose the anti-symmetrized orthonormal and complete solutions exist for the respective intrinsic Hamiltonians, $\hat{H}_A$ and $\hat{H}_B$, namely $\psi_{A\alpha}$ and $\psi_{B\beta}$,

solving for their respective eigen-energy states ϵ_α and ϵ_β as follows

$$\hat{H}_a\psi_{A\alpha} = \epsilon_\alpha\psi_{A\alpha} \tag{3.3.3}$$

and similarly for the $\psi_{B\beta}$. Thus we may expand the total wave function in terms of the internal eigenstates of the composite nuclei, given we ignore the anti-symmetrization effect of the A + B system [43].

$$\Psi(\mathbf{r}) = \sum_{\alpha\beta} \psi_{A\alpha}(\mathbf{r}_A)\psi_{B\beta}(\mathbf{r}_B)\chi_{\alpha\beta} \tag{3.3.4}$$

where $\chi_{\alpha\beta}$ is the relative motion wave function of the systems, each with internal state α and β and $\mathbf{r}$ is the relative coordinates in the centre-of-mass reference frame. The spinless core and cluster state corresponds to the elastic channel $\alpha = \beta = 0$. Through the use of the Feschbach formalism [44; 45] , we construct a ground state projection operator $\hat{P}$;

$$\hat{P} = |\psi_{A0}\psi_{B0}\rangle \langle\psi_{A0}\psi_{B0}| \tag{3.3.5}$$

and it's compliment $\hat{Q} = 1 - \hat{P}$. The eigenvalue problem reduces to [26]

$$\left[E - \hat{P}\hat{H}\hat{P} - \hat{P}\hat{H}\hat{Q}\frac{1}{E - \hat{Q}\hat{H}\hat{Q}}\hat{Q}\hat{H}\hat{P}\right]\hat{P}\Psi = 0. \tag{3.3.6}$$

The above equation is then to be multiplied from the left $\langle\psi_{A0}\psi_{B0}|$ and integrated over coordinates of the nucleons A and B results in the following;

$$\left[E - \langle\psi_{A0}\psi_{B0}|\,\hat{H}\,|\psi_{A0}\psi_{B0}\rangle - \langle\psi_{A0}\psi_{B0}|\,\hat{H}\hat{Q}\frac{1}{E - \hat{Q}\hat{H}\hat{Q}}\hat{Q}\hat{H}\,|\psi_{A0}\psi_{B0}\rangle\right]\chi_{00} = 0, \tag{3.3.7}$$

where χ_{00} is the relative motion wave function with both nuclei in their respective ground state. Using the ground state energy of the combined system to be $\epsilon_0 = 0$, then the above reduces to;

$$\left[E - \hat{T}_0 - \langle\psi_{A0}\psi_{B0}|\,\hat{V}\,|\psi_{A0}\psi_{B0}\rangle - \langle\psi_{A0}\psi_{B0}|\,\hat{V}\hat{Q}\frac{1}{E - \hat{Q}\hat{H}\hat{Q}}QV\,|\psi_{A0}\psi_{B0}\rangle\right]\chi_{00} = 0. \tag{3.3.8}$$

The above eigenvalue problem can be represented as a SWE describing the relative

$$\left[E - \hat{T}_0 - U(r)\right]\chi_{00} = 0 \tag{3.3.9}$$

where $U(r)$ is the optical potential is defined as

$$U(r) = \langle\psi_{A0}\psi_{B0}|\,\hat{V}\,|\psi_{A0}\psi_{B0}\rangle - \langle\psi_{A0}\psi_{B0}|\,\hat{V}\hat{Q}\frac{1}{E - \hat{Q}\hat{H}\hat{Q}}\hat{Q}\hat{V}\,|\psi_{A0}\psi_{B0}\rangle \tag{3.3.10}$$

where the first term describes the ground state of the interacting nuclei and the second term is a non-local, complex, energy and spin dependent component

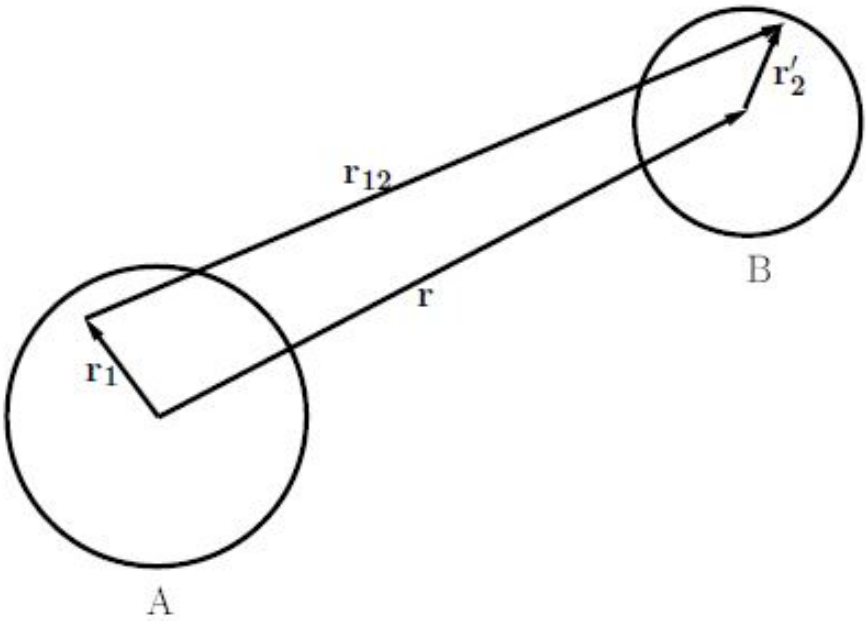

Figure 3.2: Illustration of the composite coordinate system of the folding potential [7].

[43] The folding potential of interest arises from the simplification of the first term

$$V_F(\mathbf{r}) = \int\int \rho_A(\mathbf{r_1})\rho_B(\mathbf{r_2'})v(\mathbf{r_{12}} = \mathbf{r} + \mathbf{r_2'} - \mathbf{r_1})d\mathbf{r_1}d\mathbf{r_2'} \tag{3.3.11}$$

where $\mathbf{r_1}$ and $\mathbf{r_2'}$ is the respective coordinates of nucleons 1 in the target (or core) and nucleon 2 in the projectile (or cluster) system, with the separation distance given by $\mathbf{r_{12}}$ as depicted in Figure 3.2 and the NN interaction between nucleon 1 and 2 is given by $v(\mathbf{r_{12}})$.

The anti-symmetrization of the folding potential is executed by replacing $\hat{V}$ with $(1-\hat{P}_{12})\hat{V}$ in the first term of the optical potential. Here $\hat{P}_{12}$ interchanges the coordinates between particles 1 and 2. This is equivalent to replacing $v(\mathbf{r_{12}})$ with $(1-\hat{P}_{12})v(\mathbf{r_{12}})$. Thus the folding potential simplifies as follows

$$\begin{aligned} V_F(\mathbf{r}) &= \int\int \rho_A(\mathbf{r_1})\rho_B(\mathbf{r_2'})(1-\hat{P}_{12})v(\mathbf{r_{12}})d\mathbf{r_1}d\mathbf{r_2'} && (3.3.12)\\ &= \int\int \rho_A(\mathbf{r_1})\rho_B(\mathbf{r_2'})(v(\mathbf{r_{12}}) - \hat{P}_{12}v(\mathbf{r_{12}}))d\mathbf{r_1}d\mathbf{r_2'} && (3.3.13)\\ &= \int\int \rho_A(\mathbf{r_1})\rho_B(\mathbf{r_2'})(v(\mathbf{r_{12}}) + \hat{J}(E)\delta(\mathbf{r_{12}})d\mathbf{r_1}d\mathbf{r_2'} && (3.3.14) \end{aligned}$$

in the final step $-\hat{P}_{12}v(\mathbf{r_{12}})$ is approximated by a zero range pseudo-potential[2]

[2]Sometimes also refereed to as an effective potential. These terms have been used interchangeably in various mathematics and physics literature.

$\hat{J}(E)\delta(\mathbf{r_{12}})$. By doing so, the V_F has been written into a form that reflects both the direct interaction experienced by the nucleons and the exchange of nucleons.

Nuclear densities

The ground-state density distributions of the cluster and the core are either a Gaussian parametrization for an Alpha like particle;

$$\rho(r') = 0.4299\exp(-0.7024r') \tag{3.3.15}$$

or a 2-Fermi spherically symmetric form

$$\rho(r') = \frac{\rho_0}{1+\exp((r'-c)/A)},\ c = 1.07A^{2/3}fm. \tag{3.3.16}$$

For either the core or cluster heavier than the an α particle. With ρ_0 fixed by normalizing the density to the mass number A.

3.4 Comparison between the phenomenological and M3Y potential

Within low density regions of the nucleus both the $SW + SW^3$ potential and the M3Y potential, similar characteristics are mimicked by the respective potentials. As illustrated in figure 3.3 [3]. It is in this region, commonly beyond a seperation distance of $r > 6$ fm, where the Coulomb barrier dominates. The Coulomb potential is defined in the same way for both potential models and it carries the highest contribution in determining the decay half lives.

Differences in depth and roundness of the potentials are prominent within the higher density regions, below a separation distance of 6 fm. The interior of the M3Y potential is more shallow in depth and mostly constant in the region below 4 fm, in comparison with the deeper and rounded phenomenological potential. The deeper the potential in the interior regions, the more bound states appear. Furthermore, like that of the SW and Cosh, the M3Y potential is flat in the interior giving rise to an inverted spectrum.

[3], This figure represents the $^{208}Pb{+}^{4}He$ configuration with parameters given in equation 4.3.1

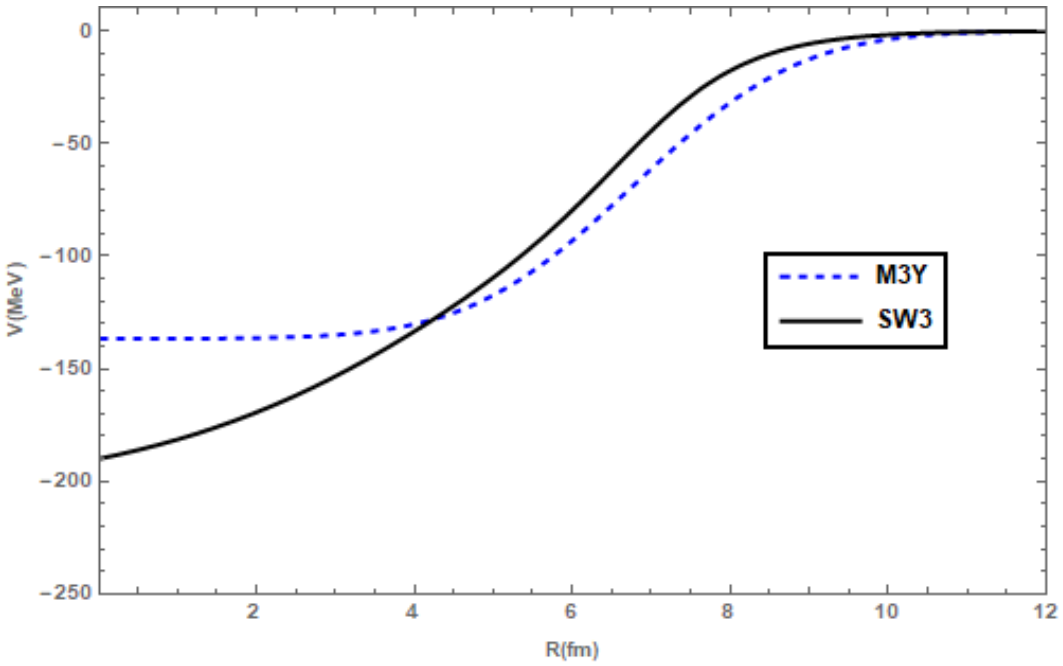

Figure 3.3: Radial plot of the Nuclear potential plus the Coulomb potential for the $^{208}Pb + ^{4}He$ configuration. The dashed line represents the M3Y form and the solid line represents the $SW + SW^3$ form of the nuclear potential.

3.5 Hybrid Potential

The M3Y interaction used within the double folding potential is derived within the nuclear scattering context, taking the following form.

$$V_{M3Y} = \lambda \int \int \rho_A(\mathbf{r_1})\rho_B(\mathbf{r'_2})(v(\mathbf{r_{12}}) + \hat{J}(E)\delta(\mathbf{r_{12}})d\mathbf{r_1}d\mathbf{r'_2} \tag{3.5.1}$$

The form of the effective interaction is fitted in such a way as to obtain a sum of 3 Yukawa terms (M3Y) [46] , ensuring single pion exchange characteristics. The form of the effective interaction $v(\mathbf{r_{12}})$ that will be used is the Reid NN potential given by [47]

$$v(\mathbf{r_{12}}) \simeq \left[7999\frac{\exp(-4r_{12})}{4r_{12}} - 2134\frac{\exp(-2.5r_{12})}{2.5r_{12}}\right] \tag{3.5.2}$$

and the exchange component $(\hat{J}(E)\delta(\mathbf{r_{12}}))$ given by

$$\hat{J}(E)\delta(\mathbf{r_{12}}) \simeq -276\left(1 - 0.005\frac{E}{A}\right)\delta(r_{12}) \tag{3.5.3}$$

with the approximations indicating the fit to the spin and isospin components of this interaction and $\frac{E}{A}$ being the bombarding energy per nucleon. This component represents the single nucleon knock-on exchange between the cluster

and core. For the simplification of numerical calculations,computation of the M3Y are carried out in the momentum space representation[28].

The emphasis of such scattering processes is at the surface interaction. As can be seen from figures 3.3 and 3.4, these double folding potentials does not account for the matter (and charge) distribution of the interior of the nucleus.

This discrepancy presents with an flat/constant potential within the interior regions. The shallow and flat potential yields an inverted spectrum, most prominently in the lower angular momentum states (see section 3.4). As a means to improve upon the current model, a Hybrid potential is to be considered. This potential is determined by a non- linear parameter fitting of the M3Y-type potential to the $SW + SW^3$ potential near the surface region, see figure 3.4. So doing, attaining the surface characteristics of the M3Y interaction as well as the structure described by the phenomenological potential model.

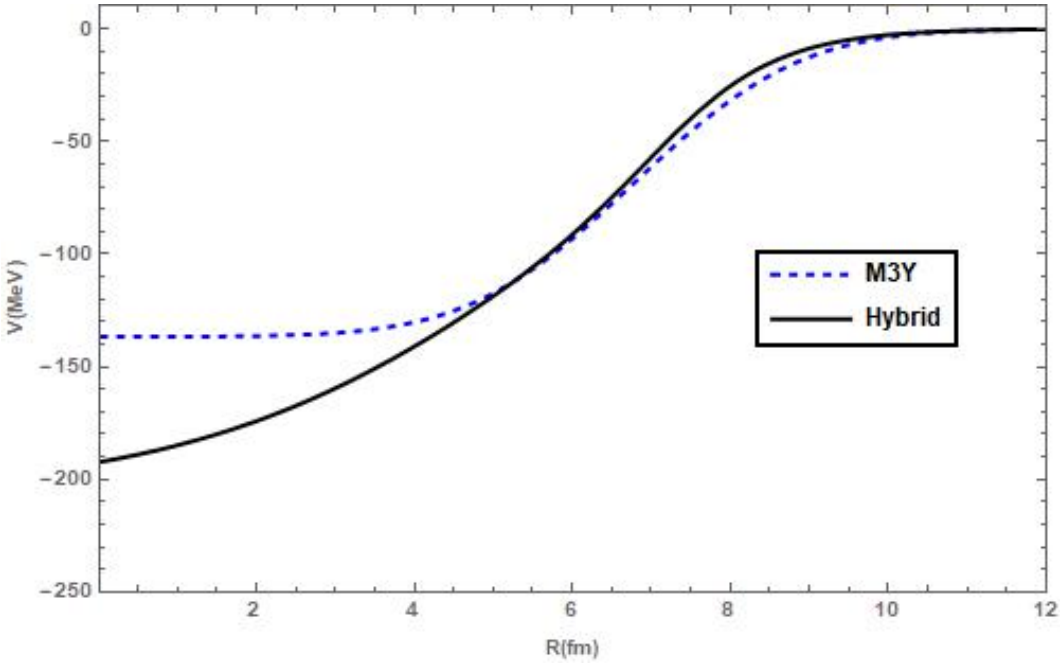

Figure 3.4: The radial plot of the M3Y potential for the $^{208}Pb+^{4}He$ configuration. Along with the phenomenological-Hybrid potential fitted to the exterior of the M3Y.

3.6 Spin considerations

In the preceding sections, the shortcoming of the $SW+SW^3$ potential is shown in that of the underbinding of the $J^\pi = 0^+$ states. This is indicative of the geometry $SW+SW^+$ potential [28]. Further corrections to the depth as given by equation 4.3.2, shown improvements to the energy of low lying states.

This section will introduce a formalism investigated by Ibrahim[28] to account for these adjustments and study the positive and negative parity states of heavy nuclei.

Excited Core Formalism

This alternative approach to the BCM, assumes the core could be in it's ground state ($I^\pi = 0^+$) or in an excited state ($I^\pi = 3^-$) with an excitation energy of $E(3^-)$. Then coupling these two states to an even or odd global quantum number (G) when studying positive or negative parity states respectively.

The formalism to follow allows for the calculation of the negative parity spectrum as well through the diagonalization of an effective Hamiltonian defined as follows:

$$\hat{H}(\mathbf{r},\hat{\xi}) = \hat{H}_0(\mathbf{r}) + \hat{H}_{int}(\xi) + V_T(\mathbf{r},\xi) \tag{3.6.1}$$

in which $\hat{H}_0(\mathbf{r})$ is the relative motion defined in chapter 1.3, $\hat{H}_{int}(\xi)$ is the core Hamiltonian with internal coordinates ξ and $V_T(\mathbf{r},\xi)$ is the non-central interaction potential coupling the cluster and core. Thus the stationary Schrödinger Wave Equation (SWE) becomes

$$\left[\hat{H}_0(\mathbf{r}) + \hat{H}_{int}(\xi) + V_T(\mathbf{r},\xi) - E\right]\Psi_{JM}(\mathbf{r},\xi) = 0 \tag{3.6.2}$$

The wave function represented above is that of the total wave function and may be expanded in terms of the coupled basis i.e. the basis of $\hat{H}_0(\mathbf{r})+\hat{H}_{int}(\xi)$;

$$\Psi_{JM}(\mathbf{r},\xi) = \sum_{L'} \alpha^J_{L'} \frac{\psi_{L'}(r)}{r} \Phi^{JM}_{L'I}(\hat{\mathbf{r}},\xi) \tag{3.6.3}$$

In the above equation, $\alpha^J_{L'}$ is the expansion coefficients, $\frac{\psi_{L'}(r)}{r}$ is the radial component of the wave function in the relative coordinates of the cluster-core system, and $\Phi^{JM}_{L'I}(\hat{\mathbf{r}},\xi)$ is the wave function obtained from the coupling of the angular part of the relative wave function to the core eigenfunction $\phi_{I\lambda}(\xi)$ such that

$$\Phi^{JM}_{L'I}(\hat{\mathbf{r}},\xi) = \sum_{\lambda,\mu} \langle L'\mu I\lambda|\,|JM\rangle\, Y_{L'\mu}(\hat{\mathbf{r}})\phi_{I\lambda}(\xi) \tag{3.6.4}$$

L' is the relative angular momentum, $I = 3$ is the angular momentum of the excited core angular momentum and with μ and λ are the projections of L' and I respectively onto the z-axis.

Using the expansion of the total wave function and inserting this form into the SWE yields; firstly applied to the relative motion

$$\hat{H}_0 \left(\sum_{L'} \alpha^J_{L'} \frac{\psi_{L'}(r)}{r} \Phi^{JM}_{L'I}(\hat{\mathbf{r}}, \xi) \right) = \sum_{L'} E_L \alpha^J_{L'} \frac{\psi_{L'}(r)}{r} \Phi^{JM}_{L'I}(\hat{\mathbf{r}}, \xi) \tag{3.6.5}$$

secondly,

$$\hat{H}_{int} \left(\sum_{L'} \alpha^J_{L'} \frac{\psi_{L'}(r)}{r} \Phi^{JM}_{L'I}(\hat{\mathbf{r}}, \xi) \right) = \sum_{L'} E(3^-) \alpha^J_{L'} \frac{\psi_{L'}(r)}{r} \Phi^{JM}_{L'I}(\hat{\mathbf{r}}, \xi) \tag{3.6.6}$$

Hereafter, the total effective Hamiltonian simplifies to

$$\sum_{L'} \left[E_{L'} + E(3^-) + V_T(\mathbf{r}, \xi) - E \right] \alpha^J_{L'} \frac{\psi_{L'}(r)}{r} \Phi^{JM}_{L'I}(\hat{\mathbf{r}}, \xi) = 0 \tag{3.6.7}$$

By pre-multiplying with $\frac{\psi_{L'}(r)}{r} \Phi^{JM}_{L'I}(\hat{\mathbf{r}}, \xi)$ and integrating over all the coordinates gives

$$\left[E_L + E(3^-) - E \right] \alpha^J_L + \sum_{L'} V^J_{LL'} \alpha^J_{L'} = 0 \tag{3.6.8}$$

This could be recast into

$$\sum_{L'} \left[[E_{L'} + E(3^-)] \delta_{LL'} + V^J_{LL'} \right] \alpha^J_{L'} = E \alpha^J_L \tag{3.6.9}$$

which illustrates the total Hamiltonian matrix (H^J) form that can be diagonalized, with matrix elements defined by $H^J_{LL'} = [E_{L'} + E(3^-)]\delta_{LL'} + V^J_{LL'}$. The interaction term is given by

$$V^J_{LL'} = \langle LI; JM | \, V_T(\mathbf{r}, \xi) \, | L'I; JM \rangle \tag{3.6.10}$$

By assuming a quadrupole-quadrupole form of the non-central interaction [48; 49]

$$V_T(\mathbf{r}, \xi) = \epsilon g(r) Y_2(\hat{r}) \cdot Y_2(\xi) \tag{3.6.11}$$

where ϵ is the tuning parameter for the strength of the spin interaction and the function $g(r)$ is related to the first derivative of the nuclear potential [49]

$$g(r) = -r \frac{\partial V_N(r)}{\partial r} \tag{3.6.12}$$

The coupling matrix evaluated with the quadrupole-quadrupole assumption gives

$$\begin{aligned} V^J_{LL'} &= \langle LI; JM | \, V_T(\mathbf{r}, \xi) \, | L'I; JM \rangle \\ &= \langle LI; JM | \, \epsilon g(r) Y_2(\hat{r}) \cdot Y_2(\xi) \, | L'I; JM \rangle \\ &= \epsilon g_{LL'} \langle Y_L I; JM | \, Y_2(\hat{r}) \cdot Y_2(\xi) \, | Y_{L'} I; JM \rangle \end{aligned} \tag{3.6.13}$$

where

$$g_{LL'} = \int \frac{\psi_L(r)}{r} g(r) \frac{\psi_{L'}(r)}{r} r^2 dr \tag{3.6.14}$$

The matrix element with respect to the angular components is a special case of the general form $\langle Y_L I; JM| \, Y_k(\hat{r}) \cdot Y_k(\xi) \, |Y_{L'} I'; J'M' \rangle$, with solution as found in [30].

$$\begin{aligned} \langle Y_L I; JM| \, Y_k(\hat{r}) \cdot Y_k(\xi) \, |Y_{L'} I'; J'M' \rangle &= \langle Y_L I; J| \, |Y_2(\hat{r}) \cdot Y_2(\xi)| \, |Y_{L'} I'; J' \rangle \, \delta_{JJ'} \delta_{MM'} \\ &= (-1)^{J-L-I'} \hat{L} \hat{I} W(LL'II'; kJ) \\ &\quad \langle Y_L| \, |Y_k(\hat{\mathbf{r}})| \, |Y_{L'} \rangle \, \langle I| \, |Y_k(\xi)| \, |I' \rangle \, \delta_{JJ'} \delta_{MM'} \end{aligned} \tag{3.6.15}$$

here $W(abcd; ef)$ is the Racah W-coefficient, which are simply a scaling of the Wigner 6-j symbol and it is this representation that will be used in the calculation of the interaction.

The special case of interest to this formalism is that for which $k = 2$, $I = I' = 3$, yielding

$$\begin{aligned} V^J_{LL'} &= \epsilon g_{LL'} \, \langle Y_L 3; JM| \, Y_2(\hat{r}) \cdot Y_2(\xi) \, |Y_{L'} 3; JM \rangle \\ &= (-1)^{J-L+L'} \epsilon g_{LL'} \frac{7}{4\pi} \hat{L} \hat{L}' W(LL'33; 2J) \\ &\quad \langle L0L'0|20\rangle \langle 3030|20\rangle \end{aligned} \tag{3.6.16}$$

Chapter 4

Calculations, Results and Observations

4.1 Introduction

In the preceding chapter[1] a variety of important nuclear potential models have been introduced, namely the phenomenological ($SW + SW^3$) potential, the M3Y double folding potential, a Hybrid-M3Y model and addressing spin correction by the Excited Core Formalism. Each of the aforementioned models has different emphasises in its description of cluster-core interaction. The $SW + SW^3$ model speaks to the global description of the structure of the nucleus, whilst the M3Y emphasis the nucleon-nucleon (NN) interaction. The comparison and suggest fix to the shortcomings of the microscopic description [2] lead to the development of a Hybrid-M3Y potential (section 3.5), utilizing the surface contribution from the M3Y and the geometry of the internal structure from $SW + SW^3$. Thus the Hybrid model shall be used ahead of the M3Y double folding interaction.

In the rest of this chapter, after brief commentary on the calculation procedure,the strengths of the $SW + SW^3$ and the Hybrid-M3Y model shall be tested on ^{212}Po under various cluster-core configurations. These various configuration shall test the formalism presented in chapter 2, all of which are to be considered as single decay processes. Clusters that will be focused on is α, ^{8}Be, ^{10}Be, ^{14}C and ^{16}O. The question this research project seeks investigate is whether these multi-alpha cluster molecules would exhibit the properties of a single collective of cluster nucleons or whether the structural properties of the subsystem of multi-alpha particles would be prominent in the structure observables of these nucleus. The choice of a fix parent nucleus gives one a systematic understanding of how the structure observables are dependent on a diminishing core size as the cluster size increases. This thesis will, however,

[1] See Chapter 3

[2] See sections 3.4

specifically focus on the ^{216}Rn to understand whether the two alpha particle configuration in this nucleus would show a strong correlation between each other and exhibit the collective property of ^{8}Be, or whether these alpha particles exhibits individual character within the parent nucleus, while sharing a common state, to form a Bose-Einstein condensate. The interaction with the more favourable fit, shall be then used in the study of the possibility or multi-clustering in ^{216}Rn. Adjustments to the nuclear interaction as a special case of the Excited core formalism shall conclude testing.

4.2 Model prediction of Observables

The first result attained from the calculation presented in chapter 2 is in fact an adjustment and not an observable. During the initialisation of the parameters of the cluster-core system, the nuclear radius is defined as $R = 1.2A^{1/3}fm$. The nuclear radius is modified iteratively as to satisfy the Born-Sommerfeld Rule as represented in equation 2.4.18, with the ground state energy being taken to be the binding energy. Hereafter, the total potential is defined with this new radius and is used in the calculations of the decay half-life, energy spectra and B(E2).

Calculation are carried out on Wolfram Mathematica [50], using a combination of built numerical methods and self coded functions. The roots and turning points of the potentials are calculated using incremental search methods, with the standard of Machine Precision being used as both accuracy and precision goals. If memory allocation does not permit this level of precision or accuracy, it is recommended to lower either to 10^{-5}.

Definite integrals, such Fourier integrals or the application of equation 2.4.18, are calculated using the Trapezoidal rule. This rule if applied to a function $F(r)$ between the bounds of a and b is as follows [51];

$$\int_a^b F(r)dr = \frac{h}{2}[F(a)+2F(a+h)+2F(r+2h)+2F(r+3h)+\cdots+F(b)] \quad (4.2.1)$$

where h is the step size which is chosen to be $10^{-3}fm$. The SE is solved using the built in `NDSolve` function, which is at its core an adaptive step-size Runge-Kutta 4^{th} order differential equation solving algorithm [51].

With these calculations being fit to the experimental results and the measure of error being used is the Root Mean Squared Error (RMSE) defined as

$$\textbf{RMSE} = \sqrt{\frac{1}{N}\sum_{n=1}^{N}\left(O_n^{Exp} - O_n^{Calc}\right)^2} \quad (4.2.2)$$

The RMSE is calculated as follows, the difference between the experimental O_n^{Exp} and calculated O_n^{Calc} observables is taken, then summed over the number

of observables from 1 to N. The mean of this sum is taken and the final metric is the squared root of the mean.

4.3 Theoretical Predictions

4.3.1 Multi-cluster analysis of Polonium 212

As a starting point for test calculations, model comparison will be done on $^{216}Po \rightarrow ^{208}Pb + ^{4}He$. This configuration is chosen as each of the components (parent nucleus, core and cluster) are doubley magic. [3]

The typical parameters used in the initiation of the calculations for the $SW + SW^3$ are [25]:

$$V_0 = 56.6A_2,\ x = 0.36,\ a = 0.76fm, \tag{4.3.1}$$

These parameters were proposed as to incorporate the existence of larger clusters within the exotic decay process. All these parameters has various effects on the nuclear structure and shall be explained in the following section 4.3.1.1. Utilising this set of parameters, allows for parameters like the potential depth, only need to be rescaled from their best fit values obtained for α decay [25; 28].

4.3.1.1 Parameter dependence in $SW + SW^3$

Although the values for the parameters stipulated, and are normally kept constant [25]the depth of the potentials may vary from $V_0 = 55.7A_2$ MeV to $V_0 = 56.6A_2$ MeV [25]. Each structural observable has different dependencies on the diffuseness, mixing parameter and the depth of the potential. The parameter dependence has been investigated by du Toit et al [7] and is summarised as follows:

1. **Radius** The nuclear radius R_0 is fitted to the Q-value of the ground state energy for every parameter configuration. Its value increases with increasing diffuseness and decreases with increasing mixing parameter and potential depth.

2. **Reduced Electromagnetic Transition Probability** The transition probability increases with increasing diffuseness parameter and decreases with increasing mixing parameter and potential depth. The sensitivity of the $B(E2)$ to parameter change is characterised by a 40% and a 4% change arising from a 10% change in the diffuseness and mixing parameters respectively. This is also seen to be the observable with least sensitivity to the change in parameters.

[3] The calculation procedure may be found in chapter A of the appendices.

3. **Exotic Decay Half Life** The half-life decreases with increasing diffuseness parameter, and increases with increasing mixing parameter and potential depth. It is most sensitive to changing parameters, specifically that of the mixing parameter and the potential depth. Where a 10% increase in either mixing parameter or potential depth can cause a change by a factor of 400 and 100.

   The dependence of the half-life on the pre-formation probability is also important. As P becomes smaller, the half-life becomes longer.

4. **Energy Spectra** The energy level increases with increasing diffuseness parameter and potential depth, while decreasing with increasing mixing parameter.

For the $SW + SW^3$ model, the chosen initiation parameters indicated by equation 4.3.1, are chosen under the above results.

As discussed in the of chapter 3, specifically 3.4, the interior regions of the M3Y below a separation distance of 4 fm is near constant/flat. These features yields an inverted spectrum for that of ^{212}Po. As such, Nucleon-Nucleon interaction as prescribed by the current microscopic model needs improvement. This is done by following the procedure stated in [47] and is achieved by performing a non-linear parameter fitting of the double folding potential to that of the $SW + SW^3$ near the surface region. Furthermore, light clusters such as ^4He and ^{10}Be require a more attractive potential near the origin as to overcome the strongly under-bound 0^+ and/or 2^+ states. Thus for configurations involving these light clusters, an additional (constant) term is added to the potential;

$$V_{corr} = \begin{cases} -V_\delta & \text{if } r \leq r_0 \\ 0 & \text{if } r > r_0 \end{cases} \tag{4.3.2}$$

with the minimum distance $r_0 \approx \frac{1.132}{A_2} fm$ according to [47].

Upon following this procedure, reveals a deepening of the potential and more tightly bound parent nucleus with a shorter nuclear radius, see table 4.3.1.1.

Table 4.1: SW3 and Hybrid potential parameter comparison for ^{212}Po.

	SW3	Hybrid
V_0	170.5 MeV	200 MeV
a_0	0.84 fm	0.83 fm
x	0.33	0.33
R	7.622 fm	7.056 fm

In the next sections, configurations based on a fixed parent and fixed (stable) core will be explored and how the proposed nuclear interactions alludes to clustering predictions.

4.3.2 Fixed Parents Nucleus Analysis

Experimental results affirm that ^{212}Po achieves stability by the emission of the light cluster of ^{4}He. Commonly known as the α of ^{212}Po to the more ^{208}Pb. At this point, two other alternative configurations will be considered, in which the mass of the cluster is increased while maintaining the mass of the parent nuclei. This increase in cluster mass is done to determine the possibility of a heavier cluster existing in the parent nuclei of interest.

Table 4.2: Energy spectra(in MeV) comparison for ^{212}Po for the phenomenological $(SW + SW^3)$ model.

	Core	^{208}Pb	^{204}Hg	^{198}Pt
	Cluster	^{4}He	^{8}Be	^{14}C
L^π	E_L^{Exp}	E_L^{Calc}		
0^+	0.	0.294	(-0.274)	(-0.237)
2^+	0.727	0.719	0.005	-0.060
4^+	1.133	1.008	0.211	0.107
6^+	1.356	1.368	0.503	0.341
8^+	1.476	1.793	0.840	0.636
10^+	1.834	2.216	1.233	0.985
12^+	2.702	2.618	1.657	1.384
14^+	2.886	2.921	2.114	1.828
16^+		3.060	2.579	2.314
18^+	2.922	2.924	3.058	2.838
$RMSE$		0.5971	0,8583	0,9638

From table 4.2 it should be noted for ^{212}Po, experimental data for 16^+ is not known.

Both alternative configurations presents with under-binding in its ground state. All of which increases gradually up to the 8^+ , with a sudden rise thereafter. This decrease in mass asymmetry, even if just a slight decrease, changes the diffuseness of the parent nuclei. Which leads to a compression in the spectra within the lower angular momentum regions. For the $^{208}Pb + \alpha$ predicts that the energy for the 16^+ is higher than 18^+. Suggesting that the gap in the experimental data could be attributed to these two states being close to one another and thus hard to distinguish between the two states.

M3Y fixed parent observations

It should be noted that the system involving M3Y microscopic model has a direct and exchange component of within its potential, $V_{M3Y}(r) = \lambda(V_D + V_{Ex})$. This potential is calculated through an iterative process, using the Q-value as the ground state energy. The known classical turning points are determined and the normalisation parameter λ is optimised iteratively until equation 2.4.18 is satisfied. Once the Bohr-Sommerfeld Quantization Rule is satisfied, V_{M3Y} is fitted to a $SW + SW^3$ potential.

The resultant energy spectra obtained from the hybrid potential (See table 4.3), shows a similar trend as the pure phenomenological potential. Namely, either a higher or lower ground state energy and slow increasing energies below the $J^\pi = 8^+$ state. With the alternate configurations having a significantly low energy than the observed α-decay.

Table 4.3: Energy spectra (in MeV) comparision for ^{212}Po for the M3Y model

	Core	^{208}Pb	^{204}Hg	^{198}Pt
	Cluster	^{4}He	^{8}Be	^{14}C
L^π	E_L^{Exp}	E_L^{Calc}		
0^+	0.	(5.562)	(6.502)	(-0.237)
2^+	0.727	0.898	1.128	-0.060
4^+	1.133	0.479	0.249	0.107
6^+	1.356	0.740	0.306	0.341
8^+	1.476	1.182	0.511	0.636
10^+	1.834	1.725	0.783	0.985
12^+	2.702	2.303	1.111	1.384
14^+	2.886	2.865	1.478	1.828
16^+		3.337	1.863	2.314
18^+	2.922	3.618	2.269	2.838
$RMSE$		0.3915	0.9487	0.9339

4.3.3 Multi-clustering of Radon 216

In chapter 4, many properties and meaningful observations were made with ^{208}Pb as a stable core and, ^{212}Po as parent nuclei. With all these analysed across multiple nuclear cluster-core models. However, these same principles and models are transferable to the investigation of higher order fission modes, e.g. ternary fission.

This is the aim of this chapter, to compare the properties of ^{216}Rn as a configuration of $^{212}Po + \alpha$ or $^{208}Pb +^{8} Be$. In so doing, we can gain insight into which configuration is more favourable both structurally and in terms of its break up.

4.3.4 Phenomenological $SW + SW^3$ model

Following the same initialization parameters and procedure as used in chapter 4; the global quantum number $G = 5A_2$ [52] Both the configurations' depth and radii are dependant on the cluster mass A_2. Along with an optimal depth parametrisation determined to be $V_0 = 54.7A_2$. This yields a depth of 218.8 MeV and 437.6 MeV respectively.

Table 4.4 is a level scheme comparison of the experimental observation and the calculated values. Regardless of the increased depth in the potential associated with the ^{8}Be cluster, the lower angular momentum states is strongly compressed up to the 8^{+} state. The resulting model comparison yields a root mean squared error of 0.30992 and 0.78541 respectively.

Table 4.4: Energy spectra (in MeV) comparision for ^{216}Rn for the phenomenological model.

	Core	^{208}Pb	^{204}Hg
	Cluster	^{4}He	^{8}Be
L^{π}	E_L^{Exp}	E_L^{Calc}	
0^+	0.	0.232	0.255
2^+	0.461	0.254	0.258
4^+	0.841	0.270	0.241
6^+	1.226	0.826	0.305
8^+	1.645	1.419	0.800
10^+	1.940	1.999	1.287
12^+	2.406	2.578	1.721
14^+	2.826	3.115	2.209
16^+	3.238	3.530	2.708
18^+	3.572	3.743	3.230

One should recall that the calculations is done in the center of mass coordinate system. As shown in the proceeding chapter, the slight change in the mass asymmetry increases the sensitivity to the diffuseness parameter of within the $SW + SW^3$ potential.

Table 4.5: Dipole transition (in MeV) comparision for ^{216}Rn for the phenomenological model

Core	^{212}Po	^{208}Pb
Cluster	^{4}He	^{8}Be
$2^+ \rightarrow 0^+$	5.75	20.22
$4^+ \rightarrow 2^+$	8.95	30.06
$6^+ \rightarrow 4^+$	9.50	33.96
$8^+ \rightarrow 6^+$	9.01	34.86
$10^+ \rightarrow 8^+$	8.19	34.30
$12^+ \rightarrow 10^+$	7.11	33.67
$14^+ \rightarrow 12^+$	5.83	32.69
$16^+ \rightarrow 14^+$	4.42	31.40
$18^+ \rightarrow 16^+$	2.95	29.83

Table 4.5 is a list of calculated $B(E2; L_i \rightarrow L_f)$, quadrupole transition strengths for the positive parity ground state band for the ^{216}Rn candidates. With the larger cluster candidate values than that of the ^{4}He, being 4 times in the lower angular momentum transitions and 9 times larger when nearing the $J^{\pi} = 18^+$ state. This can be attributed to the doubling of the cluster charge.

The theoretical half-life is calculated using the adjusted radius, after the Bohr-Sommerfield quantization is taken in to account and assuming the ground state decay energy to be that of the Q-value.

4.3.5 Microscopic M3Y hybrid model

The Michigan 3-Yukawa or M3Y potential form used is given by

$$V_{M3Y} = \lambda \int \int \rho_A(\mathbf{r_1})\rho_B(\mathbf{r'_2})(v(\mathbf{r_{12}}) + \hat{J}(E)\delta(\mathbf{r_{12}})d\mathbf{r_1}d\mathbf{r'_2} \tag{4.3.3}$$

This equation is a density dependent nuclear potential. Calculated with the Reid potential model given by equation 3.5.2 and 3.5.3. Although the densities of the core in either configuration share the same analytical form, their clusters does not. For α clusters are given a Gaussian parametrization

$$\rho_{^4He}(r) = 0.4299\exp(-0.7024r)$$

whilst heavier cluster like that of the ^8Be in question is calculated using a 2 parameter Fermi distribution such as

$$\rho_{Be}(r) = \frac{\rho_0}{1+\exp\left(\frac{r-R_{Be}}{a}\right)} \tag{4.3.4}$$

with the radius being initialised as $R_{Be} = 1.07A^{1/3}$.

The calculations are done within the momentum space through the application of a Fourier transform of the M3Y potential3.5.1

$$\overline{V}_{M3Y}(\mathbf{q}) = \int \exp(i\mathbf{q}\cdot\mathbf{r})V_{M3Y}(r)d\mathbf{r}. \tag{4.3.5}$$

Using the above Fourier transform representation and applying it to the effective interaction gives the following

$$\begin{aligned}
\overline{V}_{M3Y}(\mathbf{q}) &= \int\int\int \exp(i\mathbf{q}\cdot\mathbf{r})\rho_A(\mathbf{r_1})\rho_B(\mathbf{r'_2})v(\mathbf{r_{12}})d\mathbf{r}d\mathbf{r_1}d\mathbf{r'_2} \\
&= \int\int\int \exp(i\mathbf{q}\cdot(\mathbf{r_{12}}+\mathbf{r_1}-\mathbf{r'_2}))\rho_A(\mathbf{r_1})\rho_B(\mathbf{r'_2})v(\mathbf{r_{12}})d\mathbf{r_{12}}d\mathbf{r_1}d\mathbf{r'_2} \\
&= \int \exp(i\mathbf{q}\cdot\mathbf{r_1})\rho_A(\mathbf{r_1})d\mathbf{r_1}\int \exp(-i\mathbf{q}\cdot\mathbf{r'_2})\rho_B(\mathbf{r'_2}d\mathbf{r'_2})\int \exp(i\mathbf{q}\cdot\mathbf{r_{12}})v(\mathbf{r_{12}})d\mathbf{r_{12}} \\
&= \overline{\rho_A}(\mathbf{q})\overline{\rho_B}(-\mathbf{q})\overline{v}(\mathbf{q})
\end{aligned} \tag{4.3.6}$$

where $\overline{\rho_A}(\mathbf{q})$, $\overline{\rho_B}(-\mathbf{q})$ and $\overline{v}(\mathbf{q})$ are the respective momentum space representation of the nuclear densities $\rho_A(\mathbf{r_1})$, $\rho_B(\mathbf{r'_2})$ and the effective NN interaction $v(\mathbf{r_{12}})$. Taking the inverse Fourier transform

$$\begin{aligned}
V_{M3Y} &= \frac{1}{(2\pi)^3}\int \exp(-i\mathbf{q}\cdot\mathbf{r})\overline{V}_{M3Y}(\mathbf{q})d\mathbf{q} \\
&= \frac{1}{(2\pi)^3}\int \exp(-i\mathbf{q}\cdot\mathbf{r})\overline{\rho_A}(\mathbf{q})\overline{\rho_B}(-\mathbf{q})\overline{v}(\mathbf{q})d\mathbf{q}
\end{aligned} \tag{4.3.7}$$

Which are numerically easier to compute than equation 3.5.1. The final potential used in the calculations of the observables is a hybrid potential or more aptly, a non- linear parameter fitting of the M3Y potential onto a $SW + SW^3$ equation.

In general, the calculated is energy levels presented in table 4.6 from the resulting interaction and calculation procedure are too strongly compressed within the lower angular momentum region. The depth of the 18^+ state is deeper than models or even the lower angular states of this models.

Table 4.6: Energy spectra (in MeV) comparison for ^{216}Rn for the Hybrid/M3Y model.

	Core	^{208}Pb	^{204}Hg
	Cluster	^{4}He	^{8}Be
L^π	E_L^{Exp}	E_L^{Calc}	
0^+	0.	(5.231)	(5.172)
2^+	0.461	0.262	0.260
4^+	0.841	0.263	0.209
6^+	1.226	0.243	0.214
8^+	1.645	0.409	0.242
10^+	1.940	1.096	0.263
12^+	2.406	1.653	0.243
14^+	2.826	2.217	0.578
16^+	3.238	2.727	1.214
18^+	3.572	**31.673**	1.693

4.3.6 Excited Core formalism

In section 3.6 an adjustment to the cluster model is suggested in the form of a modification that incorporates spin interactions. Here we will calculate the spectrum with this interaction of ^{216}Rn with the assumption that the radial integral $g_{LL'}$ are similar for all L, L' [48] and is then approximated by a constant value of g. This simplifies this changes the strength parameter as follows

$$\beta = \frac{\epsilon g}{4\pi} \tag{4.3.8}$$

The assumption is true if the ground state radial wave functions are very similar.

Positive Parity

For the positive parity calculations, a stable core and cluster is considered. Even though this formalism was intended to attempt the calculation of the negative parity states through the an energy excitation and the angular momentum coupling, in these results, the cluster and core are assumed to be in it's ground state. This is in accordance with the assumptions stated in section 3.6, in the same procedure is followed but, instead coupling 2 $J^\pi = 0^+$ states (of cluster and core) to a even G value. Thus this application used is a special case within the formalism, the study negative parity states is not covered within the scope of this study and shall be presented within future work. This then results in a significantly closer, but higher energy fit throughout the spectra. With a root mean squared error of 0.0349311, which is a tenth of that the phenomenological description.

	E_{Exp}	E_{Calc}
0^+	0.	0.056
2^+	0.461	0.510
4^+	0.841	0.881
6^+	1.226	1.260
8^+	1.645	1.674
10^+	1.940	1.969
12^+	2.406	2.431
14^+	2.826	2.850
16^+	3.238	3.260
18^+	3.572	3.595

Table 4.7: The positive energy spectra (in MeV) comparison for ^{216}Rn calculated with the Excited Core Formalism.

4.4 Final Remarks

The M3Y model is a microscopic potential with nucleon- nucleon interaction. Given the form of interaction chosen, the effects are most prominent along the surface of the nuclei in question. It does not take into account any medium effects(interactions between internal nucleons) occurring inside the cluster or core.

The structure of the M3Y model can be simplified to being made up of a direct and an exchange potential, simplified to the following form;

$$V_{M3Y} = \lambda(V_D + V_{Ex}) \tag{4.4.1}$$

where λ is a normalization parameter. In calculation, a momentum space calculation of the unscaled potential is made then, it is transformed to coordinate space where it is the scaled as to adhere to the 2.4.18. This result is what is fitted to the $SW + SW^3$ potential, more specifically fitted along the exterior region beyond the first turning point of the potential.

As a result, the potential and results thereof is a mere approximation of the interaction along the surface of the nuclei and not a complete picture of the interactions.

Chapter 5

Conclusion

The $SW + SW^3$ and M3Y-hybrid potentials have been used to study heavy doubly nuclei, with a variety of test parent nuclei explored. A doubly closed ^{208}Pb as a stable core with ^{4}He as starting point for study. The mass asymmetry of the parent nuclei is then decreased as a means to study the parameter optimization of the various cluster-core interactions. Test results in chapter 4 were compared with a fixed parent of ^{212}Po and an study of varying parents through the use of a fixed core with ^{208}Pb. So doing show it's versatility whilst being applied to ^{212}Po, ^{218}Rn and ^{228}Th. Preliminary results from the two models were compared and shown that the $SW + SW^3$ model produced a better reproduction of the available experimental data. Thus the multi-cluster analysis focused on the $SW + SW^3$ model.

Radon 216 application

In chapter 4.3.3, these models are used as a technique to investigate the possibility of a higher order or multi-stage fission process. With $^{212}Po + \alpha$ being the binary fission or decay process, the second process is that of $^{208}Pb +^{8} Be$ is to represent the equivalent 3 body process for $^{208}Pb + 2\alpha$. In the comparison of the phenomenological and hybrid potentials, both models overestimate of the ground state with the hybrid potential being significantly higher. The $SW + SW^3$ potential underestimates the spectra for J^{π} from 2^{+} to 8^{+}. Whilst the M3Y yields inconsistencies throughout the spectra, suggesting a lifting in the potential that is not coherent with a realistic nuclear structure. Calculated quadrupole transition strengths $B(E2 : J_i \rightarrow J_f)$, see table 4.5, suggests that the ^{8}Be or 2 α is energetically favoured. The experimental half-life of ^{216}Rn is 45 μs, calculated half-lives various vastly. With the alpha cluster having a half life of 20 μs, which is of the correct order of magnitude but, that attributed to ^{8}Be is of the of years more aptly 10^{26} years.

Even though the ^{8}Be cluster decay is possible and more energetically favoured by calculated $B(E2 : J_i \rightarrow J_f)$, the energy spectra and half-life

corresponding to the alpha decay has a smaller error. With 2 of the 3 observables affirms that, even though the ^8Be decay process is possible, observing the alpha decay process is more probable.

It should be noted that the total potential is assumed to be separable into the nuclear cluster-core potential, Coulomb potential and the angular momentum contribution. The Schrödinger equation (SE) is solved in the coupled basis and regardless, the potential only mentions the total angular momentum and not the tensor coupling of the individual angular momentum which is mentioned in chapter 3.6. In order to simplify calculations the radial wave-functions of the cluster-core relative motion are considered to be similar. Incorporating these changes addresses the angular momentum dependent fluctuation in the observables. When applied to the calculation of the energy spectra of the favoured alpha decay, the individual changes brought to each energy level reduced the total RMSE to within a tenth of the previous value when no momentum coupling is considered.

5.1 Summary of observations made

5.1.1 Procedural Observations

1. The effective NN M3Y-hybrid interaction potential lack of well defined medium effects and scaling procedure of the exchange and direct interactions shows a significant underestimates in energies for $J^\pi \leq 8^+$.

2. Based on both proceeding chapters, the more successful model is the phenomenological $SW + SW^3$ model

3. As a choice of parametrization for the potential should take the following in consideration for varying cluster mass (A_2);

   - If the $A_2 = 4$, the starting initialisation of the diffuseness **a** is to start at 0.86 fm
   - If $A_2 > 4$, the advised value of the diffuseness is $0.56fm \leq a \leq 0.76fm$

   This is a result of the diffused interaction between the cluster and core.

4. The increase in cluster mass (A_2) presents with the following changes in the interested observables;

   - The ground state 0^+ is underbound and requires further corrections by the deepening of the potential
   - Quadrupole transitions $B(E2)$ values increase immensely, alluding to an energetic expulsion of these clusters.

- Calculated half lives $T_{1/2}$ for these configurations goes from nanoseconds or seconds range to the order of years. Often and more simply put, to an improbable observational time.

5. Finally, the use of the procedure described in appendix A and then, calculate the observable as set out by the Excited Core Formalism

5.1.2 Nuclei Specific Observations

1. Experimental and calculated values for ^{212}Po agrees that the likely decay mechanism would be as follows $^{212}Po \rightarrow ^{208}Pb + ^{4}He$

2. Furthermore, the experiment data for the $J^{\pi} = 16^{+}$ is not known and by my calculation the predicted energies should be about 3.060 MeV.

3. The multi-cluster investigation of ^{216}Rn could be interpreted in two ways. Firstly, a single alpha particle expulsion or alpha decay of ^{216}Rn is the more likely mode of decay. Secondly, the high $B(E2)$ values and the difference to the single alpha decay could mean that the ^{216}Rn is likely to undergo a 2-stage alpha decay in short succession.

5.2 Suggestions for Future work

With a forthcoming fits of the proposed configurations for ^{212}Po and ^{216}Rn, the predictions and observations requires experimental verification. For ^{212}Po, the energy of the 16^{+} is not known. With challenges in attaining this angular momentum state and it's short half life, requires a different approach to study this state. A study of other reaction mechanisms to approach this desired state is needed.

Configurations within the fixed core calculations, created parents nuclei of polonium, radon and thorium, all of which can be considered as possible multi-alpha cluster systems. For $n\alpha + ^{208}Pb$, in which the above represents n equal 1, 2 and 3 respectively. A more in depth study within this family of $n\alpha + ^{208}Pb$ systems needs to be undertaken, both experimentally and theoretically.

Appendices

Appendix A

Numerical Procedure

Analytical solutions to the radial Schrödinger equation (RWE) with an arbitrary potentials are not always possible. The RWE is a 2^{nd} order differential equation given as follows;

$$\left(-\frac{\hbar^2}{2\mu}\frac{d^2}{dr^2}+V(r)\right)\varphi_{nL}(r)=E_{nL}\varphi_{nL}(r). \tag{A.0.1}$$

Which is then separated into two coupled first order differential equations;

$$\begin{aligned}\frac{d\varphi}{dr} &= \psi(r)\\ \frac{d^2\varphi}{dr^2}=\frac{d\psi}{dr} &= -k^2(r)\psi(r)\end{aligned} \tag{A.0.2}$$

where k is the wave number and is given by $k^2(r)=\frac{2\mu}{\hbar^2}(E-V(r))$ An appropriate (adaptive and/or stiff) Runge-Kutta method will be used to solve for $\varphi(r)$.

The total potentials involved in this thesis are separated into the nuclear potential, Coulomb potential and the angular momentum contribution. The Coulomb and angular momentum potentials are central potentials i.e. inversely proportional to the separation distance r , and as such blows up at the origin. With initial conditions for this system of equations is then chosen to be as follows: $\varphi(10^{-5}=0)$ and $\varphi'(10^{-5})=0.148$.

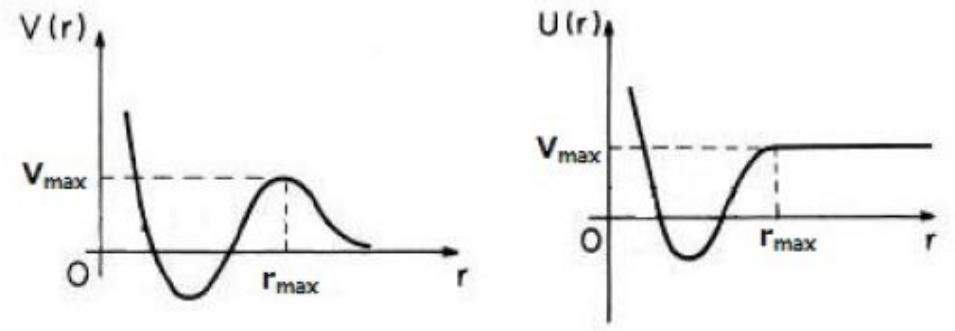

Figure A.1: The nuclear potential V(r) (left) vanishes for larger radial distances. The modified potential U(r) (right) has a constant potential beyond the point r_{max} [7].

A.1 Coding Procedure

1. Define Constants and hyper-parameters
   Such as atomic masses, reduced mass, Q-value, Global Quantum number, etc.
2. Define the potential
3. Import experimental energy data
4. Adjust the depth of the nuclear potential to satisfy the Born-Sommerfeld equation 2.4.18 for the ground state energy.
5. Determine the separation distance that maximises the total potential, label as r_{max}
6. Store the list of maximum potentials per angular momentum value
7. To avoid producing an unbound wave-function, the total potential is modified as is shown in figure A.1.

$$U(r) = \begin{cases} V_N + V_C + V_L & \text{if } r < r_{max} \\ V_{max} & \text{if } r > r_{max} \end{cases} \tag{A.1.1}$$

8. Determine the roots (matching points) of the modified potential
9. Solve the Schrödinger equation for the solutions greater and lower than r_{max}
10. Continuity of the wave-function
11. Find the energy Eigen-values of each solution

Appendix B

Fixed Core Configuration

Here the choice of a stable core is ^{208}Pb. With clusters of ^{4}He, ^{10}Be and, ^{16}O, these configurations are representative of ^{212}Po, ^{218}Rn and ^{228}Th respectively.

Phenomenological calculations

1. Polonium-212
   This is a configuration of Pb-208 and an alpha nuclei
   Q = 8.985 MeV, G = 18 V0= 170.50 MeV, a0 = 0.84 fm, x=0.33, R = 7.65692 fm
   calculated $T_{1/2} = 4.5ns$

Table B.1: Experimental and calculated energy spectra comparison in MeV.

	E_{Exp}	E_{Calc}
0^+	0.	0.294
2^+	0.727	0.719
4^+	1.133	1.008
6^+	1.356	1.368
8^+	1.476	1.793
10^+	1.834	2.216
12^+	2.702	2.618
14^+	2.886	2.921
16^+		3.060
18^+	2.922	2.924

Table B.2: Calculated B(E2) values in MeV.

$2^+ \rightarrow 0^+$	6.52
$4^+ \rightarrow 2^+$	10.54
$6^+ \rightarrow 4^+$	11.11
$8^+ \rightarrow 6^+$	10.84
$10^+ \rightarrow 8^+$	10.
$12^+ \rightarrow 10^+$	8.76
$14^+ \rightarrow 12^+$	7.24
$16^+ \rightarrow 14^+$	5.54
$18^+ \rightarrow 16^+$	3.73

2. Radon-218 This is a configuration of Pb-208 and an Be-10 nuclei Q = 14.36 , G = 50 V0= 547, a0 = 0.76 fm, x=0.33, R = 6.81923 fm calculated $T_{1/2} = 1.65 \times 10^{15}$ years

Table B.3: Experimental and calculated energy spectra comparison in MeV.

	E_{Exp}	E_{Calc}
0^+	0	-0.076
2^+	0.324	0.155
4^+	0.653	0.360
6^+	1.014	0.645
8^+	1.393	1.002
10^+	2.169	1.422
12^+	2.577	1.898
14^+	3.002	2.424
16^+	3.438	2.993
18^+	3.859	3.597

Table B.4: Calculated B(E2) values in MeV.

$2^+ \rightarrow 0^+$	20.37
$4^+ \rightarrow 2^+$	28.97
$6^+ \rightarrow 4^+$	31.57
$8^+ \rightarrow 6^+$	32.55
$10^+ \rightarrow 8^+$	32.77
$12^+ \rightarrow 10^+$	32.52
$14^+ \rightarrow 12^+$	31.93
$16^+ \rightarrow 14^+$	31.08
$18^+ \rightarrow 16^+$	30.02

3. Thorium-228 This is a configuration of Pb-208 and Oxygen-16
   Q = 44.723 , G = 100, P = 0.38 V0= 1094.0, a0 = 0.75 fm, x=0.36, R = 6.64487 fm
   calculated $T_{1/2} = 2.66 \times 10^{14}$ years

Table B.5: Experimental and calculated energy spectra comparison in MeV.

	E_{Exp}	E_{Calc}
0^+		-0.123
2^+	0.058	
4^+	0.187	0.126
6^+	0.378	0.307
8^+	0.623	0.539
10^+	0.912	0.817
12^+	1.239	1.139
14^+	1.600	1.501
16^+	1.988	1.903
18^+	2.408	2.341

Table B.6: Calculated B(E2) values in MeV.

$2^+ \rightarrow 0^+$	86.63
$4^+ \rightarrow 2^+$	123.32
$6^+ \rightarrow 4^+$	134.51
$8^+ \rightarrow 6^+$	139.34
$10^+ \rightarrow 8^+$	141.45
$12^+ \rightarrow 10^+$	142.11
$14^+ \rightarrow 12^+$	141.86
$16^+ \rightarrow 14^+$	140.98
$18^+ \rightarrow 16^+$	139.63

In these calculations, the increase in cluster mass causes under-binding in the ground states of the resulting nuclei. All of which presents with a root mean squared error of less than 1.2.

Bibliography

[1] von Weizsäcker, C.F.: Newer model demonstrations about the construction of atomic nuclei. conclusion. *Naturwissenschaften*, vol. 26, pp. 209â–217, April 1938.

[2] Pandharipande, V.R., Sick, I. and Huberts, P.K.d.: Independent particle motion and correlations in fermion systems. *Reviews of Modern Physics*, vol. 69, no. 3, p. 981, 1997.

[3] Trenn, T.J., Geiger, H., Marsden, E. and Rutherford, E.: The geiger-marsden scattering results and rutherford's atom, july 1912 to july 1913: the shifting significance of scientific evidence. *Isis*, vol. 65, no. 1, pp. 74–82, 1974.

[4] Rutherford, E.: Collision of α particles with light atoms. iv. an anomalous effect in nitrogen. *Philosophical Magazine*, vol. 90, no. S1, pp. 31–37, 2010.

[5] Buck, B., Merchant, A. and Perez, S.: Systematics of alpha-cluster states above double shell closures. *Physical Review C*, vol. 51, no. 2, p. 559, 1995.

[6] Bonetti, R. and Guglielmetti, A.: Cluster radioactivity: an overview after twenty years. *Romanian reports in Physics*, vol. 59, no. 2, p. 301, 2007.

[7] Du Toit, E.: Cluster model analysis of exotic decay in actinide nuclei, 2014. Unpublished thesis.

[8] Sonzogni, A.: Nndc chart of nuclides. In: *International Conference on Nuclear Data for Science and Technology*, pp. 105–106. EDP Sciences, 2007.

[9] Greiner, W.: A new insight in the decay modes of heavy nuclei. *Romanian Reports in Physics*, vol. 59, no. 2, p. 193, 2007.

[10] Fink, H., Maruhn, J., Scheid, W. and Greiner, W.: Theory of fragmentation dynamics in nucleus-nucleus collisions. *Zeitschrift fuer Physik*, vol. 268, no. 3, pp. 321–331, 1974.

[11] Maruhn, J. and Greiner, W.: The asymmetrie two center shell model. *Zeitschrift für Physik*, vol. 251, no. 5, pp. 431–457, 1972.

[12] Martin, B.: *Nuclear and particle physics*. John Wiley and Sons Pty. Ltd., 2006.

[13] Wagemans, C.: *The nuclear fission process*. CRC press, 1991.

[14] Beck, C., Papka, P., Zafra, A.S.I., Thummerer, S., Azaiez, F., Bednarczyk, P., Courtin, S., Curien, D., Dorvaux, O., Goasduff, A. *et al.*: Clusters in light nuclei. In: *XLV Zakopane Conference on Nuclear Physics" Extreme of the Nuclear Landscape"*, vol. 42, pp. 747–756. 2010.

[15] Poenaru, D., Nagame, Y., Gherghescu, R. and Greiner, W.: Systematics of cluster decay modes. *Physical Review C*, vol. 65, no. 5, p. 054308, 2002.

[16] Sandulescu, A., Poenaru, D. and Greiner, W.: New type of decay of heavy nuclei intermediate between fission and. cap alpha. decay. *Sov. J. Particles Nucl.(Engl. Transl.);(United States)*, vol. 11, no. 6, 1980.

[17] Rose, H. and Jones, G.: A new kind of natural radioactivity. *Nature*, vol. 307, no. 5948, p. 245, 1984.

[18] Wildermuth, K. and Kanellopoulos, T.: The âcluster modelâ of the atomic nuclei. *Nuclear Physics*, vol. 7, pp. 150–162, 1958.

[19] Buck, B., Dover, C. and Vary, J.: Simple potential model for cluster states in light nuclei. *Physical Review C*, vol. 11, no. 5, p. 1803, 1975.

[20] Griffiths, D.: *Introduction to Quantum Mechanics*. Pearson international edition. Pearson Prentice Hall, 2005. ISBN 9780131118928.

[21] Arfken, G.: *Mathematical methods for physicists*. Academic Press, 1985. ISBN 9780120598205.

[22] Buck, B., Merchant, A. and Perez, S.: α decay calculations with a realistic potential. *Physical Review C*, vol. 45, no. 5, p. 2247, 1992.

[23] Zettili, N.: *Quantum Mechanics: Concepts and Applications*. Wiley, 2009. ISBN 9780470026786.

[24] Langer, R.E.: On the connection formulas and the solutions of the wave equation. *Physical Review*, vol. 51, no. 8, p. 669, 1937.

[25] Buck, B., Merchant, A. and Perez, S.: *Phys. Rev. Lett*, vol. 76, no. 380, 1996.

[26] Wong, S.S.: *Introductory nuclear physics*. John Wiley & Sons, 2008.

[27] Alder, K. and Steffen, R.: The electromagnetic interaction in nuclear spectroscopy ed wd hamilton. 1975.

[28] Ibrahim, T.T.: A cluster study of the nuclei ^{212}po and ^{218}rn, 2009. Unpublished thesis.

[29] Zare, R.: *Angular Momentum: Understanding Spatial Aspects in Chemistry and Physics*. John Wiley and Sons, 1988.

[30] Brink, D.M. and Satchler, G.R.: *Angular Momentum*. Oxford University Press, New York, 1993.

[31] Buck, B., Merchant, A. and Perez, S.: Coexistence of very dissimilar cluster bands in 212po. *Journal of Physics G: Nuclear and Particle Physics*, vol. 30, no. 2, p. 65, 2004.

[32] Buck, B., Merchant, A. and Perez, S.: Ground state to ground state alpha decays of heavy even-even nuclei. *Journal of Physics G: Nuclear and Particle Physics*, vol. 17, no. 8, p. 1223, 1991.

[33] Gurvitz, S. and Kalbermann, G.: Decay width and the shift of a quasistationary state. *Physical review letters*, vol. 59, no. 3, p. 262, 1987.

[34] Gurvitz, S.: Novel approach to tunneling problems. *Physical Review A*, vol. 38, no. 4, p. 1747, 1988.

[35] Lovas, R.G., Liotta, R., Insolia, A., Varga, K. and Delion, D.: Microscopic theory of cluster radioactivity. *Physics reports*, vol. 294, no. 5, pp. 265–362, 1998.

[36] Mang, H.: Alpha decay. *Annual Review of Nuclear Science*, vol. 14, no. 1, pp. 1–26, 1964.

[37] Buck, B., Merchant, A. and Perez, S.: New look at α decay of heavy nuclei. *Physical review letters*, vol. 65, no. 24, p. 2975, 1990.

[38] Seal, H.: Msc thesis, 2006. Unpublished thesis.

[39] Tariq, A.S.B., Rahman, A., Das, S., Mondal, A., Uddin, M., Basak, A., Gupta, H.S. and Malik, F.: Potential description of anomalous large angle scattering of α particles. *Physical Review c*, vol. 59, no. 5, p. 2558, 1999.

[40] Buck, B., Merchant, A. and Perez, S.: Alpha-cluster structure in po 212. *Physical review letters*, vol. 72, no. 9, p. 1326, 1994.

[41] Buck, B., Merchant, A., Perez, S. and Tripe, P.: Diffuse well analysis of exotic decay of heavy nuclei. *Physical Review C*, vol. 47, no. 3, p. 1307, 1993.

[42] Buck, B., Merchant, A., Perez, S. and Tripe, P.: Calculation of exotic decay half-lives for all observed cases. *Journal of Physics G: Nuclear and Particle Physics*, vol. 20, no. 2, p. 351, 1994.

[43] Satchler, G.R. and Love, W.G.: Folding model potentials from realistic interactions for heavy-ion scattering. *Physics Reports*, vol. 55, no. 3, pp. 183–254, 1979.

[44] Feschbach, H.: Unified theory of nuclear reactions. *Annals of Physics*, vol. 5, no. 4, pp. 357–390, 1958.

[45] Feschbach, H.: Unified theory of nuclear reactions. *Annals of Physics*, vol. 19, no. 2, pp. 287–313, 1962.

[46] G. Bertsch, J. Borysowicz, H.M. and Love, W.G.: *Nucl. Phys.*, vol. A284, no. 399, 1977.

[47] Ibrahim, T., Wyngaardt, S. and Kaya, B.K.: Analysis of the clustering in 212po, 218rn and 232u. *Nuclear Physics A*, vol. 966, pp. 73–81, 2017.

[48] Buck, B., Merchant, A. and Perez, S.: Negative parity bands in 238u. *Journal of Physics G: Nuclear and Particle Physics*, vol. 34, no. 9, p. 1985, 2007.

[49] Baldock, R.A., Buck, B. and Rubio, J.A.: Alpha cluster states in 16o. *Nuclear Physics A*, vol. 426, no. 2, pp. 222–252, 1984.

[50] Inc., W.R.: Mathematica, Version 10.0.
Available at: `https://www.wolfram.com/mathematica`

[51] Gilat, A. and Subramaniam, V.: *Numerical Methods for Engineers and Scientists*. Wiley, 2013. ISBN 9781118554937.

[52] Buck, B., Merchant, A. and Perez, S.: Exotic clustering in 232,234,236,238 u. *Nuclear Physics A*, vol. 625, no. 3, pp. 554–564, 1997.